

Ultracool white dwarfs and the age of the Galactic disc^{*}

A. Gianninas^{1†}, B. Curd¹, John R. Thorstensen², Mukremin Kilic¹,
P. Bergeron³, Jeff J. Andrews⁴, Paul Canton¹, and M. A. Agüeros⁴

¹*Homer L. Dodge Department of Physics & Astronomy, University of Oklahoma, 440 W. Brooks St, Norman, OK 73019, USA*

²*Department of Physics and Astronomy, Dartmouth College, 6127 Wilder Laboratory, Hanover, NH 03755, USA*

³*Département de Physique, Université de Montréal, C.P. 6128, Succ. Centre-Ville, Montréal, QC H3C 3J7, Canada*

⁴*Department of Astronomy, Columbia University, 550 West 120th Street, New York, NY 10027, USA*

Accepted 2015 March 8. Received 2015 March 6 1; in original form 2015 February 4

ABSTRACT

We present parallax observations and a detailed model atmosphere analysis of 54 cool and ultracool ($T_{\text{eff}} < 4000$ K) white dwarfs (WDs) in the solar neighbourhood. For the first time, a large number of cool and ultracool WDs have distance and tangential velocities measurements available. Our targets have distances ranging from 21 pc to > 100 pc, and include five stars within 30 pc. Contrary to expectations, all but two of them have tangential velocities smaller than 150 km s^{-1} thus suggesting Galactic disc membership. The oldest WDs in this sample have WD cooling ages of 10 Gyr, providing a firm lower limit to the age of the thick disc population. Many of our targets have uncharacteristically large radii, indicating that they are low-mass WDs. It appears that we have detected the brighter population of cool and ultracool WDs near the Sun. The fainter population of ultracool CO-core WDs remain to be discovered in large numbers. The Large Synoptic Survey Telescope should find these elusive, more massive ultracool WDs in the solar neighbourhood.

Key words: techniques: photometric – stars: atmospheres – stars: evolution – white dwarfs – Galaxy: disc

1 INTRODUCTION

Given the finite age of the Universe, the first asymptotic giant branch stars that formed now live as $\log(L/L_{\odot}) = -4.5$ white dwarfs (WDs; Mestel 1952; Iben & Tutukov 1984; Winget et al. 1987; Liebert, Dahn & Monet 1988; Fontaine, Brassard & Bergeron 2001). Such WDs have temperatures below 4000 K (hence classified as ultracool) and they have been observed in deep *Hubble Space Telescope* (*HST*) images of the halo globular clusters M4 and NGC 6397 (Hansen et al. 2004, 2007). The oldest WDs in these two clusters are ≈ 11.5 Gyr old.

Large-scale surveys such as the Sloan Digital Sky Survey (SDSS; Gates et al. 2004; Harris et al. 2006, 2008; Kilic et al. 2006, 2010; Vidrih et al. 2007; Hall et al. 2008), the UKIRT Infrared Deep Sky Survey (UKIDSS; Leggett et al. 2011; Catalán et al. 2012; Tremblay et al. 2014) and SuperCOSMOS (Hambly et al.

1999; Rowell, Kilic & Hambly 2008) have identified the analogues of these ultracool WDs in the field. Since these field WDs are relatively bright compared to the globular cluster WDs, optical and infrared photometry in several bands can be easily obtained from ground-based telescopes, enabling us to model their spectral energy distributions (SEDs) accurately. This is important for understanding the different opacity sources in these stars, deriving reliable temperatures and ages, and also calibrating the faint WD sequences of globular clusters that usually rely on two filter photometry.

The spectra of hydrogen-rich cool and ultracool WDs differ from those of their warmer counterparts because they show the effects of the red-wing of the $\text{Ly}\alpha$ opacity in the blue (Kowalski & Saumon 2006) and the collision-induced absorption (CIA) due to molecular hydrogen in the near-infrared (Hansen 1999). The latter shifts the peak of the SEDs of ultracool WDs back to the optical wavelengths. Unfortunately, there are only three ultracool WDs in the field with parallax measurements. These are WD 0346+246¹, SDSS J110217.48+411315.4 (here-

^{*} This work is based on observations obtained at the MDM Observatory, operated by Dartmouth College, Columbia University, Ohio State University, Ohio University, and the University of Michigan.

[†] E-mail: alexg@nhn.ou.edu

¹ We note that this object is also known as WD 0343+247.

after J1102; Kilic et al. 2012, and references therein) and LHS 3250 (Bergeron & Leggett 2002). The first two stars have SEDs that peak near $1 \mu\text{m}$. On the other hand, the LHS 3250 SED peaks at $0.6 \mu\text{m}$, representing an extreme case of CIA flux deficit in the optical and infrared. Bergeron & Leggett (2002) performed a detailed model atmosphere analysis of LHS 3250 and demonstrated that LHS 3250 has a helium-rich composition, it is overluminous, and undermassive. The best-fitting model and the parallax measurement indicate a mass of only $0.23 M_{\odot}$ (Bergeron & Leggett 2002). This is somewhat problematic as all previously known low-mass WDs are DAs with hydrogen-rich atmospheres.

Gates et al. (2004) and Harris et al. (2008) as well as several other groups have identified about a dozen stars with SEDs similar to LHS 3250. In this paper, we present parallax measurements and a model atmosphere analysis of 54 cool WDs, including half a dozen ultracool WDs and several other cool WDs with significant infrared flux deficits. Our targets were selected from the cool and ultracool WD samples of Gates et al. (2004), Vidrih et al. (2007), Harris et al. (2008) and Kilic et al. (2010), and are biased towards WDs with significant infrared flux deficits. Parallax measurements allow us to accurately determine the distances, masses and consequently the cooling ages for these stars. Section 2 outlines our observations including a description of our Bayesian approach to estimating distances. Section 3 describes the models used in our analyses followed by our results in Section 4. In Section 5, we discuss the ages and membership of the WDs in our sample as well as the implications of our results towards our understanding of WD evolution and we conclude in Section 6.

2 OBSERVATIONS

2.1 Parallax

All our parallax data are from the 2.4m Hiltner telescope at Michigan-Dartmouth-MIT (MDM) Observatory on Kitt Peak, Arizona. We used a thinned SITE CCD (named ‘echelle’); at the $f7.5$ focus, each $24 \mu\text{m}$ pixel subtended 0.275 arcsec, giving a field of view 9.4 arcmin^2 . For all our parallax data, we used a 4-inch-square Kron–Cousins I -band filter, which did not vignette the CCD. Exposure times varied with the brightness of the object, but were typically a few hundred seconds. Our data were taken on numerous observing runs between 2007 and 2011. Table 1 gives the epochs that each star was observed, and the number of exposures at each epoch.

Our reduction and analysis procedures differed only slightly from those described by Thorstensen (2003) and Thorstensen, Lépine & Shara (2008). As in the previous work, we corrected our raw parallaxes to absolute using colour-based distance estimates for the reference stars, and estimated uncertainties using the formal errors of the fit and the scatter of the reference stars. In order to correct for differential colour refraction (DCR), we need to know the colour of both the programme star and the reference stars. In previous work we measured the colours, but for this work we used SDSS $g-i$ colours and adjusted the DCR correction factor slightly to account for this. Thorstensen

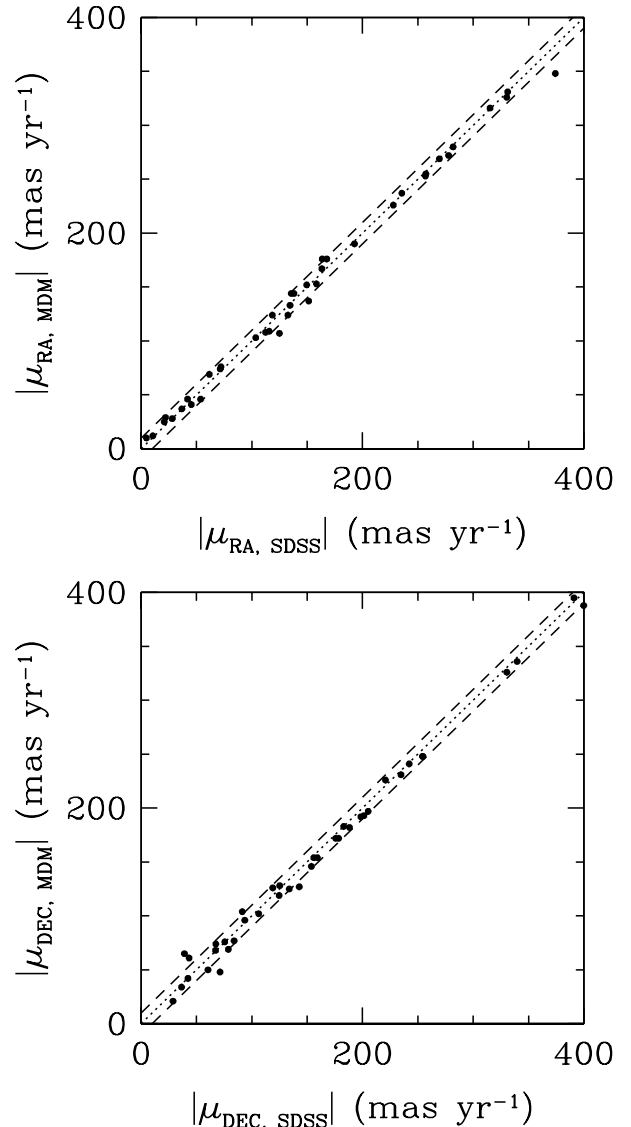


Figure 1. Comparison between the proper motions measured at MDM Observatory and those from the SDSS+USNO-B catalogue (Munn et al. 2004) for 42 of the 54 WDs in the current sample. We compare the absolute value of the proper motion in right ascension ($|\mu_{\text{RA}}|$, top) and in declination ($|\mu_{\text{DEC}}|$, bottom). The dotted line represents the 1:1 correlation. The dashed lines represent the $\pm 10 \text{ mas yr}^{-1}$ range.

(2003) describes a Bayesian procedure used to estimate distances from the available data, which combines the parallax measurement with an assumed space velocity distribution and absolute magnitude range. We used a similar approach here, but modified the prior information to be appropriate to the present sample. For the velocities, we used a composite distribution consisting of 60 per cent thin disc with $(U, V, W) = (39, 20, 20) \text{ km s}^{-1}$, 30 per cent thick disc with $(U, V, W) = (46, 50, 35) \text{ km s}^{-1}$ (Chiba & Beers 2000), and a 10 per cent probability of a still larger dispersion $(U, V, W) = (100, 75, 50) \text{ km s}^{-1}$. The absolute magnitudes of these WDs are likely to be in the range 11–18, so the absolute magnitudes were assumed to be drawn from a Gaussian centred on $M_g = 15$ with a standard deviation of 4 mag.

Table 1. Journal of parallax observations.

SDSS	N_{ref}	N_{meas}	N_{pix}	Epochs
J0045+1420	30	57	50	2007.73(4), 2007.82(3), 2008.69(11), 2008.88(16), 2008.97(8), 2009.72(8)
J0121-0038	15	48	115	2007.73(8), 2008.05(10), 2008.69(16), 2008.88(17), 2008.97(9), 2009.73(13), 2009.86(18), 2010.01(10), 2011.75(9), 2011.94(5)
J0146+1404	35	54	107	2007.73(8), 2008.05(8), 2008.69(12), 2008.88(18), 2008.97(8), 2009.73(12), 2009.86(16), 2010.01(12), 2011.75(3), 2011.94(10)
J0256-0700	15	41	149	2007.74(33), 2007.81(12), 2008.05(8), 2008.69(13), 2008.88(14), 2009.03(10), 2009.73(8), 2009.86(12), 2010.02(7), 2011.75(10), 2011.93(22)
J0301-0044	25	58	102	2007.73(7), 2007.82(6), 2008.06(8), 2008.69(10), 2008.88(17), 2008.97(8), 2009.73(12), 2009.86(13), 2010.01(12), 2011.75(9)
J0309+0025	17	47	126	2007.74(8), 2007.81(10), 2008.05(8), 2008.69(1), 2008.88(14), 2008.97(7), 2009.72(8), 2009.86(16), 2010.02(13), 2011.75(16), 2011.93(25)

(*Note.* This table is available in its entirety in a machine-readable form in the online journal. A portion is shown here for guidance regarding its form and content.)

In most cases our parallaxes were accurate enough that the Bayesian adjustments were fairly minor. Furthermore, we have four targets in common with the USNO Parallax programme and the parallax measurements are in good agreement (Harris, private communication).

There is only one target in our parallax sample, J1547+0523 (NLTT 41210), that does not display significant parallax. This object was identified as a high proper motion target by Lépine & Shara (2005), and included in our sample as a WD candidate. We measure relative proper motions of -150.5 ± 1.1 and -133.9 ± 1.1 mas yr $^{-1}$ in RA and DEC, respectively. These are consistent with the proper motion measurements by Lépine & Shara (2005). We also measure a parallax of 1.9 ± 1.4 mas, which indicates that NLTT 41210 is not a WD.

2.2 Proper Motion

In Fig. 1, we compare our measured proper motions, as listed in Table 2, for the 42 WDs in our sample that also have measured proper motions in the SDSS+USNO-B catalogue (Munn et al. 2004). We expect disagreement at the 10 mas yr $^{-1}$ level since our proper motions are relative to the particular reference stars used in the reduction. Fig. 1 shows that the vast majority of our WDs do indeed fall within the range of ± 10 mas yr $^{-1}$ when compared with the SDSS+USNO-B measurements.

This disagreement arises due to two main factors. First, we make no attempt to reduce proper motions to an inertial frame. Any systematic trend due to e.g., Galactic rotation or solar motion, is still present. Secondly, reference stars often have detectable proper motions of their own, so in μ_{RA} versus μ_{DEC} space they form a cloud of points around the origin. Because there are typically only a couple of dozen reference stars, the centre of this cloud is statistically uncertain, typically of the order of 5 mas yr $^{-1}$.

2.3 Optical and Infrared Photometry

We have obtained the available *ugriz* photometry from the SDSS Data Release 10 (DR10, Ahn et al. 2014) for the 54 WDs in our sample. These data are listed in columns two through six in Table 3 along with their uncertainties. The

majority of our targets also have near-infrared photometry available from Kilic et al. (2010), and are also listed in Table 3. For the six WDs without near-infrared photometry from Kilic et al. (2010), we adopt the near-infrared photometry from the UKIDSS Large Area Survey (ULAS) Catalog (Lawrence et al. 2007), and the Two Micron All Sky Survey (2MASS; Skrutskie et al. 2006); see the notes at the bottom of Table 3.

2.4 Optical Spectroscopy

The majority of our targets were selected from the cool WD samples of Kilic et al. (2006, 2010), hence they have optical spectroscopy obtained at the McDonald Observatory 2.7m telescope, Hobby-Eberly Telescope, or the Multiple-Mirror Telescope. The ultracool WDs and a few other cool WDs have spectroscopy available in the SDSS or the literature (Leggett et al. 2011; Giammichele, Bergeron & Dufour 2012; Tremblay et al. 2014). There are only eight DA WDs in our sample, with the rest of the stars classified as DC due to the absence of H α absorption. This overabundance of DC WDs is due to our selection bias for targeting cool and ultracool WDs.

3 THEORETICAL FRAMEWORK

Our model atmospheres and synthetic spectra are derived from the local thermodynamic equilibrium (LTE) model atmosphere code originally described in Bergeron, Saumon & Wesemael (1995) and references therein, with recent improvements discussed in Tremblay & Bergeron (2009). In particular, we now rely on their improved calculations for the Stark broadening of hydrogen lines with the inclusion of non-ideal perturbations from protons and electrons – described within the occupation probability formalism of Hummer & Mihalas (1988) – directly inside the line profile calculations. Convective energy transport is taken into account following the ML2/ $\alpha = 0.7$ prescription of the mixing length theory. Non-LTE effects are also included at higher effective temperatures but these are irrelevant for the purpose of this work. More details regarding our helium-atmosphere models are provided in Bergeron et al. (2011).

Table 2. Astrometry of cool WDs.

SDSS	RA (J2000) (h:m:s)	Dec. (J2000) (d:m:s)	π_{abs} (mas yr ⁻¹)	μ_{RA} (mas yr ⁻¹)	μ_{DEC} (mas yr ⁻¹)	D (pc)	v_{tan} (km s ⁻¹)	U^a (km s ⁻¹)	V (km s ⁻¹)	W (km s ⁻¹)
J0045+1420	00:45:21.89	+14:20:45.3	15.9 ± 1.1	251	-52	66 ⁺⁶ ₋₅	80 ± 6	-46 ± 5	-37 ± 4	-5 ± 2
J0121-0038	01:21:03.00	-00:38:33.6	9.6 ± 1.9	107	61	118 ⁺²⁹ ₋₂₁	69 ± 14	-46 ± 12	4 ± 5	27 ± 4
J0146+1404	01:46:29.01	+14:04:38.2	11.0 ± 1.5	255	65	90 ⁺¹⁴ ₋₁₀	112 ± 14	-82 ± 13	-37 ± 8	49 ± 6
J0256-0700	02:56:41.62	-07:00:33.8	16.4 ± 1.5	348	-193	61 ⁺⁶ ₋₅	115 ± 10	-17 ± 3	-96 ± 10	34 ± 3
J0301-0044	03:01:44.09	-00:44:39.5	13.4 ± 1.3	107	-538	74 ⁺⁷ ₋₆	192 ± 16	83 ± 7	-155 ± 17	-60 ± 7
J0309+0025	03:09:24.87	+00:25:25.3	21.2 ± 1.6	-10	-102	49 ⁺⁴ ₋₄	24 ± 1	23 ± 2	-3 ± 3	-4 ± 2
J0310-0110	03:10:49.53	-01:10:35.3	7.1 ± 1.9	-28	-77	164 ⁺⁵⁸ ₋₃₅	64 ± 18	47 ± 11	-14 ± 10	-25 ± 10
J0747+2438N ^b	07:47:21.56	+24:38:47.7	18.4 ± 1.0	139	-69	55 ⁺³ ₋₃	40 ± 2	29 ± 2	-13 ± 3	32 ± 3
J0747+2438S ^b	07:47:23.50	+24:38:23.7	18.4 ± 1.0	139	-69	55 ⁺³ ₋₃	40 ± 2	29 ± 2	-13 ± 3	32 ± 3
J0753+4230	07:53:13.28	+42:30:01.6	36.2 ± 1.0	108	-388	27 ⁺¹ ₋₁	53 ± 1	10 ± 1	-40 ± 2	10 ± 1
J0805+3833	08:05:57.62	+38:33:44.1	47.6 ± 1.0	-628	-552	21 ⁺¹ ₋₁	83 ± 1	-24 ± 1	-30 ± 1	-55 ± 2
J0817+2822	08:17:51.52	+28:22:03.1	19.6 ± 1.5	69	-197	52 ⁺⁴ ₋₄	51 ± 3	25 ± 2	-36 ± 4	9 ± 2
J0821+3727	08:21:08.18	+37:27:38.3	12.8 ± 3.2	167	-146	86 ⁺²⁹ ₋₁₉	90 ± 25	44 ± 8	-50 ± 16	50 ± 11
J0825+5049	08:25:19.70	+50:49:20.1	20.4 ± 1.3	-331	-326	49 ⁺³ ₋₃	108 ± 6	-48 ± 4	-51 ± 5	-57 ± 4
J0854+3503	08:54:43.33	+35:03:52.7	15.7 ± 1.5	-144	-172	64 ⁺⁷ ₋₆	68 ± 6	-14 ± 3	-37 ± 6	-32 ± 4
J0909+4700	09:09:14.56	+47:00:17.5	16.6 ± 1.7	-124	-172	61 ⁺⁷ ₋₆	61 ± 6	-17 ± 3	-36 ± 6	-16 ± 3
J0942+4437	09:42:44.96	+44:37:43.1	11.7 ± 1.2	-144	-182	87 ⁺¹⁰ ₋₈	96 ± 9	-30 ± 5	-66 ± 9	-23 ± 4
J1001+3903	10:01:03.42	+39:03:40.5	11.6 ± 2.1	-291	-175	87 ⁺¹⁹ ₋₁₃	140 ± 25	-73 ± 16	-75 ± 16	-60 ± 12
J1107+4855	11:07:31.38	+48:55:23.0	20.9 ± 1.7	-730	-69	48 ⁺⁴ ₋₄	167 ± 13	128 ± 12	-56 ± 6	-53 ± 5
J1115+0033	11:15:36.97	+00:33:15.3	20.2 ± 2.5	56	-246	51 ⁺⁶ ₋₆	61 ± 7	50 ± 5	-27 ± 5	-14 ± 3
J1117+5010	11:17:08.63	+50:10:33.9	21.3 ± 1.7	176	-126	48 ⁺⁴ ₋₄	49 ± 4	51 ± 4	1 ± 2	31 ± 2
J1158+0004	11:58:14.52	+00:04:58.3	28.9 ± 1.7	-25	183	35 ⁺² ₋₂	31 ± 1	-7 ± 2	33 ± 2	20 ± 1
J1203+0426	12:03:28.64	+04:26:53.6	22.8 ± 2.1	-253	154	45 ⁺⁵ ₋₄	63 ± 6	-50 ± 6	13 ± 2	10 ± 1
J1204+6222	12:04:39.54	+62:22:16.4	18.3 ± 2.5	-29	-154	58 ⁺¹⁰ ₋₇	43 ± 6	16 ± 2	-22 ± 5	28 ± 3
J1212+0440	12:12:07.01	+04:40:12.0	16.0 ± 2.6	-280	-48	64 ⁺¹³ ₋₉	86 ± 14	-54 ± 11	-38 ± 9	-11 ± 3
J1238+3502	12:38:12.85	+35:02:49.1	10.0 ± 2.0	-146	-123	110 ⁺²⁶ ₋₁₉	100 ± 20	-18 ± 7	-73 ± 18	12 ± 1
J1251+4403	12:51:06.12	+44:03:03.1	22.9 ± 5.3	22	-136	63 ⁺²⁹ ₋₁₆	41 ± 14	30 ± 5	-8 ± 5	15 ± 2
J1345+4200	13:45:32.92	+42:00:44.2	27.3 ± 1.0	-190	128	36 ⁺¹ ₋₁	40 ± 1	-28 ± 2	8 ± 2	9 ± 1
J1349+1155	13:49:02.33	+11:55:11.8	35.3 ± 1.6	176	-524	28 ⁺¹ ₋₁	74 ± 3	69 ± 3	-28 ± 2	-17 ± 1
J1422+0459	14:22:25.73	+04:59:39.7	16.7 ± 2.1	-272	-50	61 ⁺⁹ ₋₇	80 ± 10	-34 ± 6	-49 ± 8	28 ± 3
J1424+6246	14:24:29.52	+62:46:17.1	21.1 ± 2.0	-269	-42	48 ⁺⁵ ₋₄	62 ± 5	-23 ± 4	-31 ± 5	33 ± 3
J1436+4332	14:36:42.78	+43:32:35.7	37.1 ± 1.2	-316	498	27 ⁺¹ ₋₁	75 ± 2	-63 ± 3	25 ± 1	9 ± 1
J1437+4151	14:37:18.15	+41:51:51.5	16.0 ± 2.2	-153	-68	66 ⁺¹² ₋₈	52 ± 7	-3 ± 3	-30 ± 6	29 ± 3
J1447+5427	14:47:01.85	+54:27:44.6	21.3 ± 3.5	-237	34	51 ⁺¹¹ ₋₈	58 ± 10	-27 ± 7	-19 ± 5	27 ± 4
J1452+4522	14:52:39.00	+45:22:38.3	11.4 ± 1.4	-46	74	95 ⁺¹⁵ ₋₁₁	39 ± 5	-25 ± 6	17 ± 4	9 ± 2
J1458+1146	14:58:48.52	+11:46:55.9	17.0 ± 1.6	-124	-96	60 ⁺⁶ ₋₅	45 ± 4	7 ± 2	-31 ± 5	16 ± 2
J1534+4649	15:34:51.02	+46:49:49.5	33.1 ± 1.8	-468	226	30 ⁺¹ ₋₁	75 ± 4	-49 ± 4	-17 ± 2	40 ± 2
J1606+2547	16:06:19.81	+25:47:02.9	22.6 ± 1.7	-226	-119	45 ⁺⁴ ₋₃	54 ± 4	13 ± 2	-33 ± 4	35 ± 3
J1615+4449	16:15:44.67	+44:49:42.5	12.1 ± 3.7	46	-231	89 ⁺⁴⁷ ₋₂₀	99 ± 37	100 ± 27	-12 ± 8	1 ± 3
J1632+2426	16:32:42.23	+24:26:55.2	22.9 ± 1.2	-12	-336	44 ⁺² ₋₂	70 ± 3	65 ± 3	-30 ± 3	-5 ± 2
J1704+3608	17:04:47.70	+36:08:47.4	21.1 ± 1.7	183	-172	48 ⁺⁴ ₋₄	57 ± 4	52 ± 4	20 ± 2	-31 ± 4
J1722+5752	17:22:57.78	+57:52:50.7	17.8 ± 1.8	-37	395	56 ⁺⁶ ₋₅	105 ± 10	-94 ± 11	16 ± 2	11 ± 2
J1728+2646	17:28:07.27	+26:46:19.2	17.2 ± 1.8	-41	-248	59 ⁺⁷ ₋₆	70 ± 7	67 ± 6	-28 ± 5	-1 ± 3
J2041-0520	20:41:28.99	-05:20:27.7	15.8 ± 1.6	-152	-21	65 ⁺⁸ ₋₆	47 ± 5	41 ± 4	3 ± 3	41 ± 4
J2042+0031	20:42:59.23	+00:31:56.6	16.0 ± 1.3	-76	-241	63 ⁺⁶ ₋₅	75 ± 6	60 ± 5	-42 ± 5	-8 ± 3
J2045-0710	20:45:57.53	-07:10:03.5	12.0 ± 1.4	-74	-125	86 ⁺¹² ₋₉	59 ± 7	49 ± 5	-31 ± 6	10 ± 3
J2118-0737	21:18:05.21	-07:37:29.1	14.5 ± 2.0	109	-127	72 ⁺¹² ₋₉	57 ± 8	3 ± 3	-23 ± 6	-34 ± 6
J2147+1127	21:47:25.17	+11:27:56.1	18.9 ± 2.0	103	-248	54 ⁺⁷ ₋₅	69 ± 7	26 ± 3	-28 ± 5	-45 ± 6
J2222+1221	22:22:33.89	+12:21:43.0	24.4 ± 1.3	703	192	41 ⁺² ₋₂	142 ± 6	121 ± 7	7 ± 1	-44 ± 3
J2239+0018A ^b	22:39:54.12	+00:18:47.3	12.2 ± 2.9	-12	122	107 ⁺⁴² ₋₂₆	62 ± 19	-8 ± 6	49 ± 9	31 ± 6
J2239+0018B ^b	22:39:54.07	+00:18:49.2	12.2 ± 2.9	-12	122	107 ⁺⁴² ₋₂₆	62 ± 19	-8 ± 6	49 ± 9	31 ± 6
J2242+0048	22:42:06.19	+00:48:22.8	14.8 ± 1.7	133	-76	70 ⁺⁹ ₋₇	51 ± 5	-13 ± 4	-17 ± 4	-24 ± 4
J2254+1323	22:54:08.64	+13:23:57.2	24.2 ± 1.6	326	-192	42 ⁺³ ₋₃	75 ± 5	-24 ± 3	-28 ± 3	-44 ± 4
J2330+0028	23:30:55.20	+00:28:52.3	18.3 ± 2.3	137	104	59 ⁺⁹ ₋₇	48 ± 6	-33 ± 6	19 ± 2	9 ± 1

^a Since we do not have any radial velocity measurements for our targets, the U component has been computed assuming $v_{\text{rad}} = 0$ km s⁻¹.^b For these two binary systems, a weighted mean was adopted in the determination of their astrometric measurements.

Table 3. Optical and near-infrared photometry of cool WDs.

SDSS	<i>u</i>	<i>g</i>	<i>r</i>	<i>i</i>	<i>z</i>	<i>Y</i>	<i>J</i>	<i>H</i>	<i>K</i>
J0045+1420	20.64 ± 0.08	19.20 ± 0.03	18.45 ± 0.03	18.20 ± 0.03	18.10 ± 0.03	–	17.24 ± 0.04	16.99 ± 0.04	16.89 ± 0.04
J0121–0038 ^a	22.82 ± 0.28	20.79 ± 0.03	19.74 ± 0.03	19.38 ± 0.03	19.18 ± 0.04	18.47 ± 0.06	18.23 ± 0.08	18.05 ± 0.09	18.10 ± 0.19
J0146+1404	21.37 ± 0.11	20.00 ± 0.03	19.39 ± 0.02	19.27 ± 0.03	19.79 ± 0.11	–	19.56 ± 0.05	20.07 ± 0.12	–
J0256–0700	20.74 ± 0.08	19.00 ± 0.02	18.13 ± 0.02	17.79 ± 0.03	17.69 ± 0.03	–	16.71 ± 0.05	16.62 ± 0.05	16.48 ± 0.06
J0301–0044	22.23 ± 0.34	20.43 ± 0.03	19.38 ± 0.02	18.99 ± 0.02	18.92 ± 0.04	–	17.96 ± 0.04	17.73 ± 0.04	17.68 ± 0.08
J0309+0025	19.15 ± 0.03	18.19 ± 0.02	17.72 ± 0.02	17.53 ± 0.02	17.50 ± 0.02	–	16.64 ± 0.04	16.54 ± 0.04	16.87 ± 0.04
J0310–0110	22.71 ± 0.30	20.89 ± 0.04	20.18 ± 0.03	19.91 ± 0.03	19.75 ± 0.08	–	18.94 ± 0.02	18.73 ± 0.02	18.58 ± 0.02
J0747+2438N	21.01 ± 0.08	19.29 ± 0.02	18.59 ± 0.02	18.23 ± 0.01	18.14 ± 0.02	–	17.16 ± 0.04	16.99 ± 0.04	16.85 ± 0.04
J0747+2438S	19.49 ± 0.03	18.37 ± 0.01	17.91 ± 0.01	17.73 ± 0.01	17.69 ± 0.02	–	16.78 ± 0.04	16.58 ± 0.04	16.53 ± 0.04
J0753+4230	19.97 ± 0.04	18.09 ± 0.01	17.19 ± 0.01	16.87 ± 0.01	16.75 ± 0.02	–	15.69 ± 0.04	15.49 ± 0.04	15.47 ± 0.04
J0804+2239	19.73 ± 0.03	18.30 ± 0.02	17.59 ± 0.01	17.39 ± 0.01	17.33 ± 0.02	–	16.71 ± 0.04	16.92 ± 0.04	17.29 ± 0.06
J0805+3833 ^b	19.00 ± 0.02	17.31 ± 0.01	16.56 ± 0.02	16.27 ± 0.02	16.20 ± 0.02	–	15.34 ± 0.05	15.19 ± 0.08	14.90 ± 0.09
J0817+2822	21.59 ± 0.16	19.49 ± 0.02	18.61 ± 0.01	18.30 ± 0.01	18.22 ± 0.03	–	17.33 ± 0.04	17.01 ± 0.04	16.91 ± 0.09
J0821+3727	20.68 ± 0.06	19.14 ± 0.02	18.43 ± 0.01	18.15 ± 0.02	18.04 ± 0.02	–	17.25 ± 0.04	17.00 ± 0.04	16.85 ± 0.05
J0825+5049	21.09 ± 0.09	19.34 ± 0.02	18.43 ± 0.02	18.09 ± 0.02	18.00 ± 0.03	–	17.08 ± 0.04	16.83 ± 0.04	16.74 ± 0.04
J0845+2257	15.57 ± 0.01	15.73 ± 0.01	16.08 ± 0.01	16.35 ± 0.02	16.61 ± 0.02	–	16.24 ± 0.11	15.96 ± 0.00	16.48 ± 0.00
J0854+3503	23.57 ± 0.67	20.53 ± 0.03	19.39 ± 0.02	19.09 ± 0.03	18.95 ± 0.05	–	18.44 ± 0.04	18.23 ± 0.04	17.98 ± 0.04
J0909+4700	20.64 ± 0.15	19.29 ± 0.03	18.74 ± 0.02	18.50 ± 0.02	18.42 ± 0.05	–	18.11 ± 0.04	18.62 ± 0.07	19.10 ± 0.10
J0942+4437	21.37 ± 0.09	19.47 ± 0.02	18.58 ± 0.01	18.22 ± 0.02	18.05 ± 0.02	–	17.15 ± 0.04	16.97 ± 0.04	16.86 ± 0.04
J1001+3903	21.36 ± 0.10	20.05 ± 0.02	19.60 ± 0.02	20.02 ± 0.03	20.61 ± 0.17	–	20.65 ± 0.06	21.05 ± 0.07	–
J1107+4855	21.50 ± 0.12	19.49 ± 0.03	18.54 ± 0.02	18.23 ± 0.02	18.11 ± 0.03	–	17.05 ± 0.05	16.95 ± 0.07	16.86 ± 0.07
J1115+0033 ^a	19.50 ± 0.04	17.92 ± 0.01	17.22 ± 0.02	16.99 ± 0.01	16.90 ± 0.02	–	15.78 ± 0.08	15.65 ± 0.18	15.59 ± 0.26
J1117+5010	21.17 ± 0.10	19.34 ± 0.03	18.57 ± 0.03	18.30 ± 0.02	18.16 ± 0.03	–	17.24 ± 0.04	17.07 ± 0.04	16.97 ± 0.05
J1158+0004	20.86 ± 0.11	18.89 ± 0.04	17.85 ± 0.02	17.54 ± 0.01	17.34 ± 0.03	–	16.36 ± 0.04	16.31 ± 0.05	16.18 ± 0.05
J1203+0426	19.57 ± 0.03	18.18 ± 0.02	17.50 ± 0.02	17.21 ± 0.01	17.12 ± 0.02	–	16.39 ± 0.01	16.49 ± 0.02	16.92 ± 0.06
J1204+6222	20.91 ± 0.09	19.25 ± 0.02	18.43 ± 0.02	18.14 ± 0.02	18.06 ± 0.03	–	17.07 ± 0.04	16.86 ± 0.04	16.80 ± 0.04
J1212+0440	22.07 ± 0.21	20.04 ± 0.03	19.09 ± 0.02	18.79 ± 0.02	18.66 ± 0.04	–	17.67 ± 0.04	17.50 ± 0.04	17.50 ± 0.05
J1238+3502	24.74 ± 0.81	21.77 ± 0.09	20.31 ± 0.06	19.88 ± 0.05	20.37 ± 0.15	–	21.19 ± 0.06	–	–
J1251+4403	21.46 ± 0.09	20.17 ± 0.03	20.39 ± 0.03	20.72 ± 0.04	20.92 ± 0.17	–	21.78 ± 0.08	–	–
J1345+4200 ^b	19.70 ± 0.03	17.85 ± 0.02	17.01 ± 0.01	16.69 ± 0.02	16.54 ± 0.01	–	15.61 ± 0.06	15.43 ± 0.11	15.00 ± 0.00
J1349+1155	20.55 ± 0.06	18.64 ± 0.02	17.84 ± 0.01	17.42 ± 0.02	17.20 ± 0.02	–	16.43 ± 0.01	16.29 ± 0.02	16.26 ± 0.02
J1422+0459	20.98 ± 0.10	19.44 ± 0.03	18.58 ± 0.02	18.27 ± 0.02	18.18 ± 0.03	–	17.15 ± 0.05	17.10 ± 0.08	17.02 ± 0.05
J1424+6246	20.38 ± 0.05	18.83 ± 0.01	18.15 ± 0.03	17.89 ± 0.02	17.71 ± 0.02	–	–	–	–
J1436+4332	19.83 ± 0.04	18.04 ± 0.02	17.19 ± 0.01	16.85 ± 0.03	16.75 ± 0.03	–	15.78 ± 0.04	15.62 ± 0.04	15.51 ± 0.04
J1437+4151	20.06 ± 0.04	19.03 ± 0.01	18.45 ± 0.02	18.23 ± 0.03	18.12 ± 0.02	–	17.43 ± 0.04	17.76 ± 0.05	18.42 ± 0.08
J1447+5427	21.23 ± 0.12	19.46 ± 0.04	18.64 ± 0.02	18.36 ± 0.02	18.25 ± 0.04	–	17.26 ± 0.07	17.20 ± 0.07	17.07 ± 0.06
J1452+4522	21.55 ± 0.10	20.01 ± 0.02	19.39 ± 0.02	19.31 ± 0.02	19.36 ± 0.06	–	18.60 ± 0.02	18.43 ± 0.02	18.37 ± 0.02
J1458+1146	20.62 ± 0.08	18.85 ± 0.02	18.02 ± 0.02	17.72 ± 0.02	17.64 ± 0.02	–	16.63 ± 0.04	16.47 ± 0.05	16.31 ± 0.06
J1534+4649	20.90 ± 0.08	18.76 ± 0.02	17.74 ± 0.02	17.36 ± 0.02	17.19 ± 0.02	–	16.17 ± 0.04	16.12 ± 0.04	16.04 ± 0.05
J1547+0523	19.96 ± 0.04	18.05 ± 0.01	17.13 ± 0.00	16.75 ± 0.00	16.51 ± 0.01	–	15.38 ± 0.00	14.95 ± 0.00	14.77 ± 0.01
J1606+2547	20.99 ± 0.08	19.24 ± 0.02	18.45 ± 0.02	18.17 ± 0.02	18.07 ± 0.04	–	17.07 ± 0.04	17.09 ± 0.06	16.84 ± 0.06
J1615+4449	21.18 ± 0.10	19.59 ± 0.02	18.84 ± 0.02	18.57 ± 0.02	18.52 ± 0.04	–	17.44 ± 0.04	17.24 ± 0.05	17.26 ± 0.07
J1632+2426	21.47 ± 0.10	19.60 ± 0.02	18.73 ± 0.02	18.49 ± 0.02	18.40 ± 0.03	–	17.67 ± 0.02	18.10 ± 0.02	18.04 ± 0.02
J1704+3608	20.50 ± 0.05	18.72 ± 0.01	17.94 ± 0.01	17.66 ± 0.01	17.55 ± 0.02	–	16.62 ± 0.04	16.34 ± 0.04	16.32 ± 0.06
J1722+5752	20.39 ± 0.06	19.28 ± 0.02	18.79 ± 0.02	18.56 ± 0.03	18.50 ± 0.03	–	17.74 ± 0.04	17.84 ± 0.05	18.75 ± 0.12
J1728+2646	19.18 ± 0.03	18.14 ± 0.02	17.68 ± 0.01	17.51 ± 0.01	17.46 ± 0.02	–	–	–	–
J2041–0520	20.95 ± 0.08	19.27 ± 0.01	18.51 ± 0.01	18.24 ± 0.01	18.14 ± 0.03	–	17.25 ± 0.04	16.97 ± 0.04	16.93 ± 0.04
J2042+0031	21.67 ± 0.14	19.95 ± 0.02	19.05 ± 0.01	18.73 ± 0.01	18.61 ± 0.03	–	17.65 ± 0.04	17.45 ± 0.04	17.36 ± 0.05
J2045–0710	21.03 ± 0.09	19.33 ± 0.02	18.60 ± 0.01	18.33 ± 0.01	18.15 ± 0.03	–	17.32 ± 0.04	17.10 ± 0.04	17.03 ± 0.04
J2118–0737	23.38 ± 0.95	20.70 ± 0.03	19.48 ± 0.03	19.01 ± 0.02	18.76 ± 0.04	–	17.90 ± 0.04	17.82 ± 0.04	17.81 ± 0.05
J2147+1127	20.83 ± 0.09	19.19 ± 0.02	18.43 ± 0.02	18.13 ± 0.02	18.01 ± 0.03	–	17.14 ± 0.04	16.84 ± 0.04	16.79 ± 0.04
J2222+1221	21.74 ± 0.11	19.48 ± 0.02	18.37 ± 0.02	17.88 ± 0.02	17.67 ± 0.02	–	–	–	–
J2239+0018A ^a	21.27 ± 0.08	20.14 ± 0.04	19.59 ± 0.03	19.48 ± 0.05	20.28 ± 0.16	19.57 ± 0.10	19.69 ± 0.19	–	–
J2239+0018B ^a	23.13 ± 0.36	20.79 ± 0.04	19.88 ± 0.03	19.49 ± 0.03	19.24 ± 0.06	18.66 ± 0.05	18.34 ± 0.06	17.98 ± 0.10	18.48 ± 0.27
J2242+0048	22.11 ± 0.22	19.63 ± 0.02	18.65 ± 0.02	18.28 ± 0.01	18.16 ± 0.03	–	18.06 ± 0.04	18.72 ± 0.07	19.16 ± 0.10
J2254+1323	21.57 ± 0.17	19.51 ± 0.02	18.49 ± 0.02	18.14 ± 0.01	18.00 ± 0.02	–	17.04 ± 0.04	16.88 ± 0.04	16.85 ± 0.04
J2330+0028	21.85 ± 0.24	19.88 ± 0.02	18.95 ± 0.02	18.66 ± 0.02	18.53 ± 0.04	–	17.63 ± 0.04	17.36 ± 0.04	17.32 ± 0.04

^a IR photometry from UKIDSS

^b IR photometry from 2MASS

Our model grid covers a range of effective temperature between $T_{\text{eff}} = 1500$ and $45,000$ K in steps of 500 K for $T_{\text{eff}} < 15,000$ K, 1000 K up to $T_{\text{eff}} = 18,000$ K, 2000 K up to $T_{\text{eff}} = 30,000$ K and by steps of 5000 K above. The $\log g$ ranges from 6.5 to 9.5 by steps of 0.5 dex, with additional models at $\log g = 7.75$ and 8.25 . We also calculated mixed hydrogen and helium atmosphere models with $\log(\text{He}/\text{H}) = -2.0$ to 5.0 , in steps of 1.0 dex.

Since the photometric technique described below relies heavily on the flux at the u and g bandpasses, we now include in our models the opacity from the red wing of Ly α (Kowalski & Saumon 2006), which significantly affects the flux in the ultraviolet.

4 PHOTOMETRIC ANALYSIS

4.1 General Procedure

Atmospheric parameters, T_{eff} and $\log g$, and chemical compositions of cool WDs can be measured accurately using the photometric technique developed by Bergeron, Ruiz & Leggett (1997). We first convert optical and infrared photometric measurements into observed fluxes and compare the resulting energy distributions with those predicted from our model atmosphere calculations. To accomplish this task, we first transform every magnitude m into an average flux f_{λ}^m . Since $ugriz$ photometry is defined

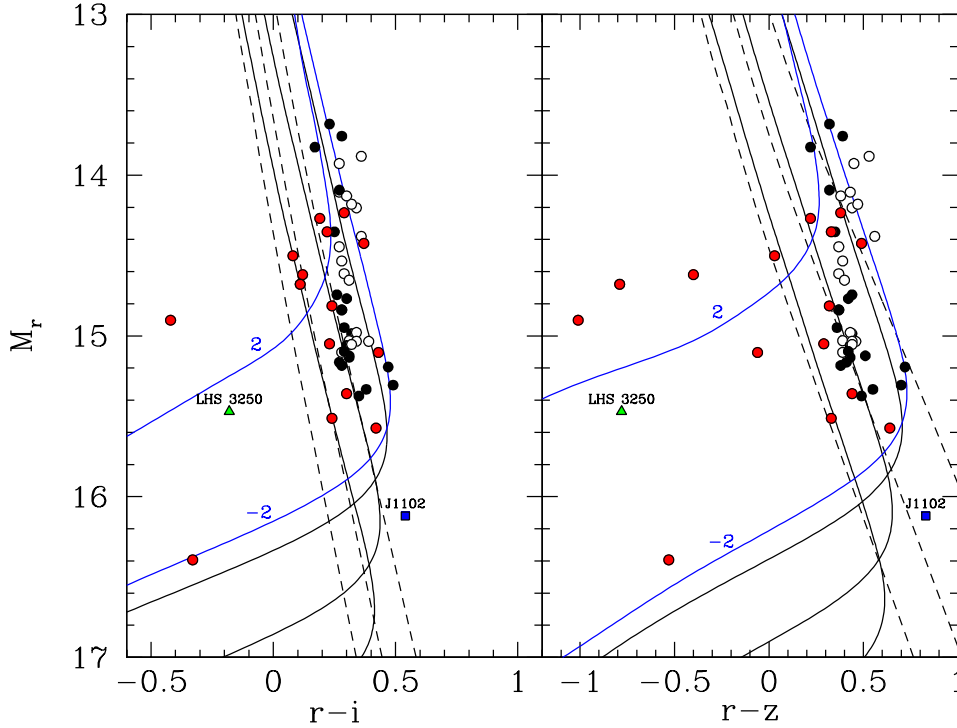


Figure 2. Location of the WDs in our sample in a M_r versus $r-i$ (left) and $r-z$ (right) colour-magnitude diagram. The black dots correspond to the WDs with H-rich atmospheres while the white dots represent the He-rich WDs. The red dots represent the 15 cool and ultracool WDs with mixed atmospheres. The solid and dashed black lines represent pure H and pure He tracks, respectively, for masses $M = 0.3, 0.6,$ and $0.9 M_{\odot}$, from right to left. The solid blue lines represent the predictions from mixed model atmospheres for $M = 0.2 M_{\odot}$. The mixed atmosphere model tracks are labelled with their He abundance $\log(\text{He}/\text{H}) = -2$ and 2 . LHS 3250 and J1102 are shown as a green triangle, and a blue square, respectively.

on the AB magnitude system, we first calculate f_{ν}^m using the equation

$$m = -2.5 \log f_{\nu}^m - 48.60 \quad (1)$$

and then f_{ν}^m is converted to f_{λ}^m following $f_{\lambda}^m = f_{\nu}^m c / \lambda^2$, where λ is the central wavelength of the given filter. For the near-infrared photometry, we obtain f_{λ}^m using the equation

$$m = -2.5 \log f_{\lambda}^m + c_m, \quad (2)$$

where c_m is a constant to be determined for each filter, as described below. In general,

$$f_{\lambda}^m = \frac{\int_0^{\infty} f_{\lambda} S_m(\lambda) \lambda d\lambda}{\int_0^{\infty} S_m(\lambda) \lambda d\lambda} \quad (3)$$

where $S_m(\lambda)$ is the transmission function of the corresponding bandpass, f_{λ} is the monochromatic flux from the star received at Earth. For the *ugriz* photometry, a slightly different definition of the above Equation (3) is required (see Equation (3) of Holberg & Bergeron 2006, for instance). The transmission functions for the *ugriz* system are described in Holberg & Bergeron (2006) and references therein. The transmission functions for the *JHK* or *JHK_S* filters on the MKO photometric system are taken from Tokunaga, Simons & Vacca (2002).

The constants c_m in Equation (2) for each passband

are determined using the improved calibration fluxes from Holberg & Bergeron (2006), defined with the *HST* absolute flux scale of Vega (Bohlin & Gilliland 2004), and appropriate magnitudes on a given system.

For each star in Table 3, a minimum set of five average fluxes f_{λ}^m is obtained, which can be compared with model fluxes. Since the observed fluxes correspond to averages over given bandpasses, the monochromatic fluxes from the model atmospheres need to be converted into average fluxes, H_{λ}^m , by substituting f_{λ} in Equation (3) for the monochromatic Eddington flux, H_{λ} . We can then relate the average observed fluxes f_{λ}^m and the average model fluxes H_{λ}^m – which depend on T_{eff} , $\log g$ and chemical composition – by the equation

$$f_{\lambda}^m = 4\pi(R/D)^2 H_{\lambda}^m \quad (4)$$

where R/D defines the ratio of the radius of the star to its distance from Earth. We then minimize the χ^2 value defined in terms of the difference between observed and model fluxes over all bandpasses, properly weighted by the photometric uncertainties. Our minimization procedure relies on the non-linear least-squares method of Levenberg–Marquardt (Press et al. 1986), which is based on a steepest decent method. Only T_{eff} and the solid angle $\pi(R/D)^2$ are considered free parameters, while the uncertainties of both parameters are obtained directly from the covariance matrix of the fit.

For stars with known trigonometric parallax measurements, we first assume a value of $\log g = 8.0$ and

determine the effective temperature and the solid angle, which combined with the distance D obtained from the trigonometric parallax measurement, yields directly the radius of the star R . The radius is then converted into mass using evolutionary models similar to those described in Fontaine, Brassard & Bergeron (2001) but with CO cores, $q(\text{He}) \equiv \log M_{\text{He}}/M_{\star} = 10^{-2}$ and $q(\text{H}) = 10^{-4}$, which are representative of hydrogen-atmosphere WDs, and $q(\text{He}) = 10^{-2}$ and $q(\text{H}) = 10^{-10}$, which are representative of helium-atmosphere WDs. After the first iteration, if $M < 0.406 M_{\odot}$, we switch to the evolutionary models of Althaus, Serenelli & Benvenuto (2001), appropriate for low-mass He-core WDs. In general, the $\log g$ value obtained from the inferred mass and radius ($g = GM/R^2$) will be different from our initial guess of $\log g = 8.0$, and the fitting procedure is thus repeated until an internal consistency in $\log g$ is reached.

4.2 Results

Fig. 2 presents the colour-magnitude diagram for our parallax sample along with the evolutionary tracks for 0.3–0.9 M_{\odot} pure H, pure He, and 0.2 M_{\odot} mixed H/He atmosphere models. Note that all the evolutionary tracks plotted in Fig. 2 represent the evolution of CO-core WDs. Two other ultracool WDs with parallax measurements and SDSS photometry, LHS 3250 and J1102 (Harris et al. 1999; Bergeron, Leggett & Ruiz 2001; Hall et al. 2008; Kilic et al. 2012), are also included for comparison.

Interestingly, the majority of the targets in our sample fall above the evolutionary tracks for 0.6 M_{\odot} WDs, indicating that they are low-mass objects. Some of these WDs are even brighter than the 0.3 M_{\odot} WD sequence, implying masses as low as $\approx 0.2 M_{\odot}$. A significant fraction of the stars in our sample are IR-faint WDs that suffer from CIA from molecular hydrogen. The CIA affects the redder optical bands and the infrared. Hence, most of these IR-faint objects lie to the left of the pure H and pure He model sequences. Note that our sample was selected to include as many IR-faint WDs as possible. Therefore, these are over-represented in this figure. It is clear from this figure that the colour-magnitude distribution of our sample is well matched by WD models with masses ≈ 0.2 –0.9 M_{\odot} with a variety of compositions, including pure H, pure He and mixed H/He atmospheres. Below we discuss the DA, DC and ultracool WD samples separately.

4.2.1 DA WDs

Fig. 3 displays the best-fitting pure-hydrogen models to the SEDs of the eight WDs classified as DA. Both the observed SEDs and the $\text{H}\alpha$ line profiles are reproduced fairly well by our pure H models. Given our parallax measurements, the best-fitting radii for these eight targets range from 0.011 to 0.022 R_{\odot} ($R > R_{\oplus}$), indicating that they are relatively low-mass WDs. In fact, half of these WDs have masses below 0.45 M_{\odot} , and therefore are likely He-core WDs. The majority of low-mass WDs are in short-period ($P \lesssim 1$ d) binary systems (Marsh, Dhillon & Duck 1995; Brown et al. 2011). Therefore, J0045+1420, J0821+3727, J1115+0033, and J1728+2646 are likely unresolved binary WDs. Table 4 provides WD cooling age estimates

for these DA WDs, as well as the rest of our parallax sample. For $M < 0.45 M_{\odot}$ WDs, we provide cooling ages for both CO and He core composition based on the evolutionary tracks of Fontaine, Brassard & Bergeron (2001) and Althaus, Serenelli & Benvenuto (2001), respectively. Regardless of the core composition, these eight DA WDs have cooling ages of less than 8 Gyr.

It is necessary to note an important caveat regarding the four potential binaries listed above. If they are indeed unresolved binaries, then the WDs in these systems will be more massive than implied by our fits assuming a single star. Hence, their actual cooling ages will be larger for a given T_{eff} . Our estimates for the cooling ages of these potential binaries should therefore be regarded, at best, as lower limits.

4.2.2 DC WDs

Fig. 4 shows our model fits to the SEDs of the 31 DC WDs that are best explained by pure H or pure He atmosphere models. In all cases, the optical spectra are featureless near the $\text{H}\alpha$ region. Hence, the choice of a pure H or pure He composition is based solely on the fits to the optical and infrared photometry. In most cases, the atmospheric parameters from both the pure H and pure He solution agree within the uncertainties. Our model fits indicate that all of these WDs have $T_{\text{eff}} < 5000$ K. The ratio of the H to He atmosphere WDs is 13/18. However, all DC WDs with temperatures below $T_{\text{eff}} = 4530$ K are best explained by H-rich atmosphere models (see also Kowalski & Saumon 2006; Giammichele, Bergeron & Dufour 2012).

Just like the DA sample discussed above, about half of the DCs in this sample are low-mass objects. The two coolest stars, J2118–0737 and J2222+1221, have $T_{\text{eff}} = 3920 \pm 60$ and 4010 ± 80 K, and $M = 0.31 \pm 0.09 M_{\odot}$ and $0.37 \pm 0.03 M_{\odot}$, respectively. Assuming He-cores, these temperatures correspond to cooling ages of 7.7 and 9.4 Gyr, respectively. If these are short-period, unresolved binary systems, then the companions would be fainter and more massive WDs. Due to the unknown prior history of such binary systems and without an estimate on their initial masses, their total ages, including the main-sequence + WD cooling ages, cannot be reliably calculated.

4.2.3 DC WDs with Mixed H/He Atmospheres

Gates et al. (2004), Harris et al. (2008) and Kilic et al. (2010) have identified several IR-faint WDs that were originally thought to be ultracool WDs with $T_{\text{eff}} < 4000$ K. It turns out that some of these IR-faint WDs are relatively warm. There are nine IR-faint, DC WDs in our sample that are best-fitted with $T_{\text{eff}} > 4500$ K mixed H/He atmospheres models. The main opacity source in these mixed models is the H_2 –He CIA in the infrared. Since cool He-rich WDs have lower opacities and higher atmospheric pressures, the CIA becomes effective at higher temperatures ($T_{\text{eff}} > 4000$ K, Bergeron & Leggett 2002).

Fig. 5 shows the SEDs for these nine DC WDs with mixed composition. The mixed models with $\log(\text{He}/\text{H}) = -0.4$ to 2.3 fit the observed SEDs (over the 0.3–2.2 μm region) fairly well. The best-fitting parameters for some of these stars are markedly different than the parameters presented in Kilic et al. (2010). However, the analysis presented

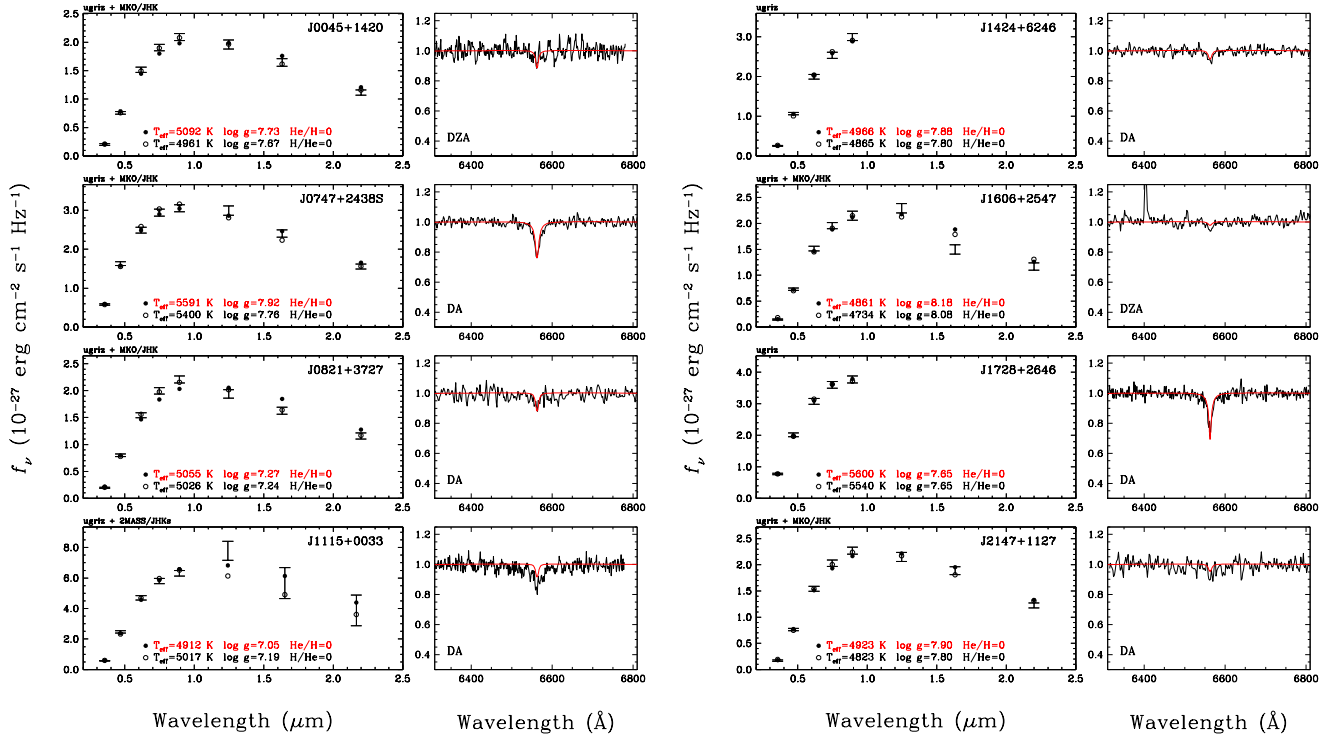


Figure 3. Fits to the observed energy distributions with pure hydrogen models (filled circles) and with pure helium models (open circles) for the eight WDs that exhibit, or potentially exhibit, absorption at $H\alpha$. Adopted atmospheric parameters are emphasized in red. Here and in the following figures, the photometric observations are represented by error bars while the filled and open circles represent the model fluxes for the pure H and pure He solution, respectively. In the right-hand panels we show the observed normalized spectra together with the synthetic line profiles calculated with the atmospheric parameters corresponding to the pure hydrogen solutions.

in this paper is superior to earlier work since we now include all available photometry in our analysis (including the u -band data) and we also have parallax measurements available. J1632+2426 is the most-massive and the oldest WD (in terms of the WD cooling age) in this sample, with a mass of $0.82 \pm 0.04 M_{\odot}$ and a cooling age of 7.7 Gyr.

4.2.4 Ultracool WDs

We originally selected 12 ultracool WD candidates for follow-up parallax observations: J0854+3503 and J1001+3903 from Gates et al. (2004); J0121–0038, J0301–0044, J2239+0018 and J2242+0048 from Vidrih et al. (2007); J0146+1404, J0310–0110, J1238+3502, J1251+4403, J1452+4522 and J1632+2426 from Harris et al. (2008). Our detailed model atmosphere analysis using parallax data shows that only half of these stars are actually ultracool WDs with $T_{\text{eff}} < 4000$ K. The rest of the ultracool candidates are best explained by pure H/He or mixed atmosphere models with $T_{\text{eff}} > 4000$ K.

Fig. 6 shows the SEDs and our model fits to the six ultracool WDs in our sample. The best-fitting parameters are given in each panel and at the end of Table 4. Note that prior to this work, there were only three ultracool WDs with parallax observations available. Hence, the ultracool WD sample presented here is a significant addition to this sample. The six ultracool WDs presented here are best explained by mixed H/He atmospheres with $T_{\text{eff}} = 2710$ –3760 K and $\log(\text{He}/\text{H}) = 0.65$ –2.96. Interestingly, all six of these ultra-

cool WDs are too bright for average mass WDs. Instead, the observed parallaxes require relatively large radii ($R = 0.015$ – $0.023 R_{\odot}$) and low masses ($M = 0.17$ – $0.39 M_{\odot}$). Assuming He-cores, the WD cooling ages range from 4.5 to 9.7 Gyr. They are located within 63–110 pc of the Sun and they display tangential velocities of 40–140 km s^{-1} . Hence, these ultracool WDs likely belong to the Galactic disc.

5 DISCUSSION

5.1 Nearby WDs

The local WD population is complete to within 13 pc, and there remains a significant number of WDs to be discovered in the solar neighbourhood (Holberg et al. 2008; Giammichele, Bergeron & Dufour 2012). Through our parallax observations, here we have uncovered WDs with distances ranging from 21 to ≈ 100 pc. Sion et al. (2014) present 224 WDs within 25 pc of the Sun. With a distance of 21 ± 1 pc, J0805+3833 (WD 0802+387) is a new addition to this sample. There are also four other WDs, J0753+4230, J1349+1155, J1436+4332 and J1534+4649, with distances ≤ 30 pc. Since parallax observations on individual targets is time consuming, significant progress on creating a complete sample of WDs in the solar neighbourhood has to wait until astrometric data from large scale surveys such as *GAIA* (Perryman et al. 2001) and the Large Synoptic Survey Telescope (LSST; Ivezić et al. 2008) become available.

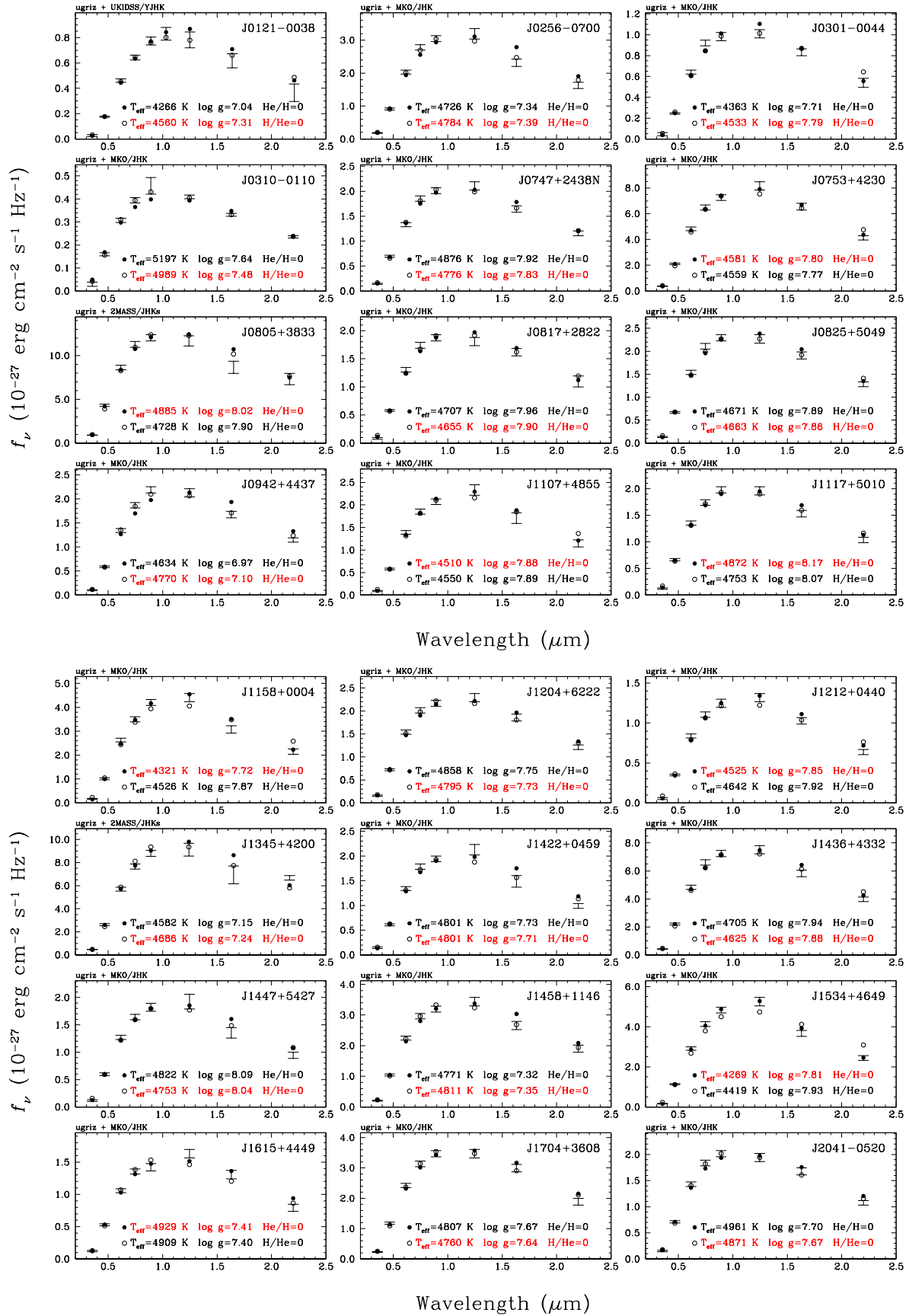


Figure 4. Fits to the observed energy distributions with pure hydrogen models (filled circles) and with pure helium models (open circles) for the 31 DC WDs. All objects have featureless spectra near the $H\alpha$ region, and the SEDs are best explained with pure model atmospheres. Adopted atmospheric parameters are emphasized in red.

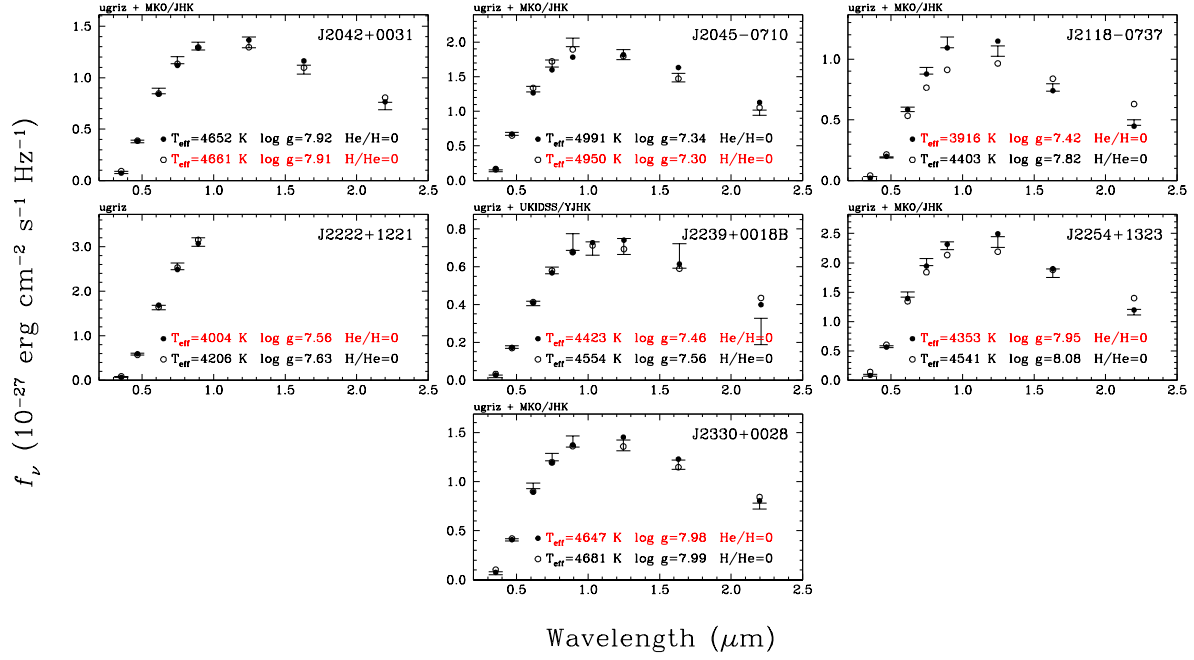
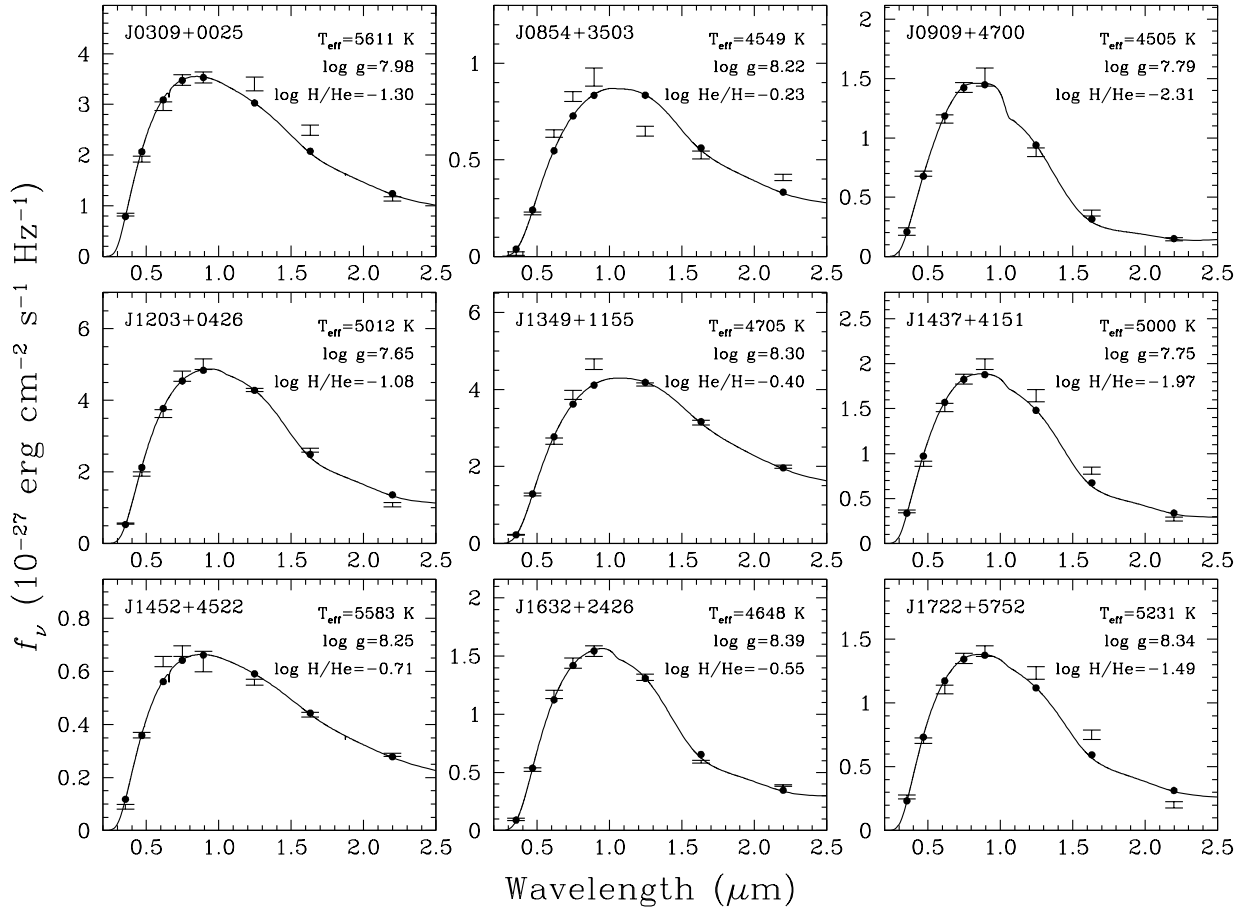
Figure 4. – *continued*

Figure 5. Fits to the SEDs of the nine IR-faint, DC WDs in our sample, excluding the ultracool WDs. All objects have featureless spectra near the $H\alpha$ region, and the SEDs are best explained with mixed model atmospheres. Note that the measured abundances are quoted relative to the dominant atmospheric constituent.

Table 4. Properties of cool WDs.

SDSS	T_{eff} (K)	$\log g$ (cm s^{-2})	M (M_{\odot})	R (R_{\odot})	Comp. (log He/H)	M_{g} (mag)	$\tau_{\text{cool,CO}}$ (Gyr)	$\tau_{\text{cool,He}}$ (Gyr)
DA								
J0045+1420	5090 ± 60	7.73 ± 0.15	0.43 ± 0.07	0.015 ± 0.001	H	15.10 ± 0.18	2.7 ^{+0.9} _{-0.6}	–
J0747+2438S	5590 ± 40	7.92 ± 0.09	0.54 ± 0.05	0.013 ± 0.001	H	14.67 ± 0.12	2.5 ^{+0.5} _{-0.3}	–
J0821+3727	5050 ± 50	7.27 ± 0.50	0.27 ± 0.15	0.020 ± 0.006	H	14.47 ± 0.59	1.6 ^{+1.0} _{-1.3}	3.1 ^{+2.4} _{-1.1}
J1115+0033	4910 ± 40	7.05 ± 0.27	0.21 ± 0.07	0.022 ± 0.003	H	14.38 ± 0.28	1.4 ^{+0.4} _{-0.7}	2.9 ^{+0.6} _{-0.6}
J1424+6246	4970 ± 60	7.88 ± 0.16	0.51 ± 0.09	0.014 ± 0.001	H	15.42 ± 0.20	4.4 ^{+1.7} _{-1.4}	–
J1606+2547	4860 ± 60	8.18 ± 0.12	0.69 ± 0.08	0.011 ± 0.001	H	15.97 ± 0.17	7.9 ^{+0.6} _{-1.1}	–
J1728+2646	5600 ± 50	7.65 ± 0.17	0.42 ± 0.07	0.016 ± 0.002	H	14.29 ± 0.24	1.6 ^{+0.4} _{-0.2}	3.5 ^{+0.8} _{-0.6}
J2147+1127	4920 ± 60	7.90 ± 0.18	0.52 ± 0.10	0.013 ± 0.002	H	15.53 ± 0.24	4.9 ^{+1.8} _{-1.8}	–
DC								
J0121–0038	4560 ± 50	7.31 ± 0.39	0.28 ± 0.13	0.019 ± 0.004	He	15.43 ± 0.46	2.2 ^{+1.1} _{-1.2}	4.6 ^{+3.2} _{-1.6}
J0256–0700	4780 ± 40	7.39 ± 0.15	0.30 ± 0.05	0.018 ± 0.002	He	15.07 ± 0.20	2.2 ^{+0.3} _{-0.3}	4.6 ^{+1.4} _{-0.9}
J0301–0044	4530 ± 50	7.79 ± 0.16	0.45 ± 0.08	0.014 ± 0.001	He	16.08 ± 0.19	4.8 ^{+1.6} _{-1.2}	–
J0310–0110	4990 ± 50	7.48 ± 0.47	0.34 ± 0.17	0.018 ± 0.005	He	14.82 ± 0.59	2.1 ^{+2.1} _{-1.1}	4.7 ^{+3.2} _{-2.0}
J0747+2438N	4780 ± 40	7.83 ± 0.10	0.47 ± 0.05	0.014 ± 0.001	He	15.59 ± 0.12	4.5 ^{+1.1} _{-0.9}	–
J0753+4230	4580 ± 40	7.80 ± 0.05	0.46 ± 0.03	0.014 ± 0.001	H	15.89 ± 0.06	5.1 ^{+0.6} _{-0.6}	–
J0805+3833	4890 ± 40	8.02 ± 0.03	0.59 ± 0.02	0.012 ± 0.001	H	15.70 ± 0.05	6.4 ^{+0.3} _{-0.4}	–
J0817+2822	4660 ± 50	7.90 ± 0.13	0.51 ± 0.08	0.013 ± 0.001	He	15.91 ± 0.17	5.6 ^{+1.5} _{-1.3}	–
J0825+5049	4660 ± 40	7.86 ± 0.11	0.49 ± 0.06	0.014 ± 0.001	He	15.89 ± 0.14	5.2 ^{+1.3} _{-1.0}	–
J0942+4437	4770 ± 40	7.10 ± 0.21	0.22 ± 0.06	0.022 ± 0.002	He	14.77 ± 0.23	1.6 ^{+0.3} _{-0.6}	3.3 ^{+0.6} _{-0.5}
J1107+4855	4510 ± 70	7.88 ± 0.14	0.50 ± 0.08	0.014 ± 0.001	H	16.08 ± 0.18	6.3 ^{+1.5} _{-1.6}	–
J1117+5010	4870 ± 60	8.17 ± 0.12	0.69 ± 0.08	0.011 ± 0.001	H	15.93 ± 0.18	7.8 ^{+0.8} _{-1.1}	–
J1158+0004	4320 ± 70	7.72 ± 0.11	0.42 ± 0.05	0.015 ± 0.001	H	16.16 ± 0.13	5.2 ^{+1.1} _{-1.0}	–
J1204+6222	4800 ± 40	7.73 ± 0.23	0.44 ± 0.11	0.015 ± 0.003	He	15.43 ± 0.31	7.2 ^{+4.3} _{-2.0}	–
J1212+0440	4530 ± 80	7.85 ± 0.29	0.49 ± 0.16	0.014 ± 0.003	H	16.01 ± 0.37	5.9 ^{+2.5} _{-2.8}	–
J1345+4200	4690 ± 20	7.25 ± 0.06	0.26 ± 0.02	0.020 ± 0.001	He	15.02 ± 0.08	2.0 ^{+0.1} _{-0.1}	4.0 ^{+0.3} _{-0.3}
J1422+0459	4800 ± 50	7.71 ± 0.24	0.41 ± 0.11	0.015 ± 0.002	He	15.51 ± 0.29	3.5 ^{+2.2} _{-1.0}	–
J1436+4332	4630 ± 30	7.88 ± 0.05	0.50 ± 0.03	0.013 ± 0.001	He	15.88 ± 0.07	5.4 ^{+0.6} _{-0.6}	–
J1447+5427	4750 ± 60	8.04 ± 0.30	0.59 ± 0.18	0.012 ± 0.003	He	15.92 ± 0.40	6.9 ^{+0.5} _{-3.5}	–
J1458+1146	4810 ± 40	7.35 ± 0.15	0.29 ± 0.05	0.019 ± 0.002	He	14.96 ± 0.20	2.1 ^{+0.3} _{-0.3}	4.2 ^{+1.3} _{-0.8}
J1534+4649	4270 ± 60	7.82 ± 0.09	0.47 ± 0.05	0.014 ± 0.001	H	16.35 ± 0.12	6.4 ^{+1.0} _{-1.0}	–
J1615+4449	4930 ± 60	7.41 ± 0.57	0.31 ± 0.18	0.018 ± 0.007	H	14.84 ± 0.74	2.0 ^{+1.9} _{-1.1}	4.3 ^{+3.3} _{-2.3}
J1704+3608	4760 ± 40	7.64 ± 0.13	0.40 ± 0.06	0.016 ± 0.001	He	15.31 ± 0.18	2.9 ^{+0.9} _{-0.4}	6.8 ^{+1.2} _{-1.1}
J2041–0520	4870 ± 40	7.67 ± 0.17	0.42 ± 0.07	0.016 ± 0.002	He	15.20 ± 0.23	2.8 ^{+1.1} _{-0.6}	6.4 ^{+1.5} _{-1.3}
J2042+0031	4660 ± 50	7.91 ± 0.15	0.52 ± 0.09	0.013 ± 0.001	He	15.95 ± 0.19	5.7 ^{+1.5} _{-1.6}	–
J2045–0710	4950 ± 40	7.30 ± 0.21	0.28 ± 0.06	0.019 ± 0.003	He	14.66 ± 0.26	1.8 ^{+0.4} _{-0.4}	3.5 ^{+1.4} _{-0.6}
J2118–0737	3920 ± 60	7.42 ± 0.25	0.31 ± 0.09	0.018 ± 0.003	H	16.41 ± 0.32	3.4 ^{+1.8} _{-0.8}	7.7 ^{+3.6} _{-2.3}
J2222+1221	4010 ± 80	7.56 ± 0.08	0.37 ± 0.03	0.017 ± 0.001	H	16.42 ± 0.11	4.2 ^{+0.9} _{-0.6}	9.4 ^{+1.3} _{-1.3}
J2239+0018B	4420 ± 90	7.46 ± 0.55	0.33 ± 0.19	0.018 ± 0.006	H	15.64 ± 0.66	2.9 ^{+3.9} _{-2.2}	6.3 ^{+7.2} _{-3.4}
J2254+1323	4350 ± 70	7.95 ± 0.12	0.54 ± 0.07	0.013 ± 0.001	H	16.39 ± 0.16	7.5 ^{+1.1} _{-1.3}	–
J2330+0028	4650 ± 80	7.98 ± 0.22	0.57 ± 0.13	0.013 ± 0.002	H	16.03 ± 0.29	6.9 ^{+1.7} _{-2.7}	–
Mixed								
J0309+0025	5610 ± 70	7.98 ± 0.13	0.56 ± 0.08	0.013 ± 0.001	1.30	14.74 ± 0.18	3.4 ^{+1.1} _{-0.8}	–
J0854+3503	4550 ± 80	8.22 ± 0.15	0.71 ± 0.10	0.011 ± 0.001	–0.23	16.50 ± 0.22	7.6 ^{+0.2} _{-0.1}	–
J0909+4700	4510 ± 110	7.79 ± 0.19	0.45 ± 0.10	0.014 ± 0.002	2.31	15.36 ± 0.23	4.8 ^{+2.0} _{-1.4}	–
J1203+0426	5010 ± 40	7.65 ± 0.16	0.41 ± 0.07	0.016 ± 0.002	1.08	14.91 ± 0.22	5.6 ^{+1.0} _{-1.0}	–
J1349+1155	4710 ± 40	8.30 ± 0.06	0.76 ± 0.04	0.010 ± 0.001	–0.40	16.37 ± 0.10	7.5 ^{+0.1} _{-0.1}	–
J1437+4151	5000 ± 70	7.75 ± 0.24	0.45 ± 0.11	0.015 ± 0.003	1.97	14.93 ± 0.32	6.2 ^{+4.9} _{-1.6}	–
J1452+4522	5580 ± 70	8.25 ± 0.20	0.73 ± 0.13	0.011 ± 0.002	0.71	15.12 ± 0.30	5.5 ^{+0.6} _{-1.5}	–
J1632+2426	4650 ± 70	8.39 ± 0.06	0.82 ± 0.04	0.010 ± 0.001	0.55	16.38 ± 0.10	7.7 ^{+0.1} _{-0.1}	–
J1722+5752	5230 ± 80	8.34 ± 0.14	0.79 ± 0.09	0.010 ± 0.001	1.49	15.54 ± 0.21	6.7 ^{+0.1} _{-0.5}	–
Ultracool								
J0146+1404	3600 ± 140	7.59 ± 0.22	0.38 ± 0.09	0.016 ± 0.003	2.82	15.23 ± 0.29	3.7 ^{+1.7} _{-1.0}	9.2 ^{+3.1} _{-3.2}
J1001+3903	2710 ± 150	7.06 ± 0.24	0.20 ± 0.09	0.022 ± 0.004	2.93	15.35 ± 0.39	2.9 ^{+2.3} _{-0.7}	7.6 ^{+4.2} _{-1.7}
J1238+3502	2900 ± 210	7.13 ± 0.42	0.22 ± 0.11	0.021 ± 0.004	0.65	16.77 ± 0.44	3.6 ^{+3.2} _{-0.1}	9.7 ^{+6.8} _{-5.0}
J1251+4403	2750 ± 180	7.67 ± 0.69	0.39 ± 0.28	0.015 ± 0.006	2.91	16.17 ± 0.73	9.1 ^{+1.4} _{-4.9}	9.1 ^{+1.3} _{-5.0}
J2239+0018A	3510 ± 220	6.95 ± 0.34	0.20 ± 0.09	0.025 ± 0.008	2.88	14.99 ± 0.66	2.0 ^{+1.8} _{-0.9}	5.2 ^{+3.7} _{-1.5}
J2242+0048	3770 ± 90	7.00 ± 0.13	0.20 ± 0.03	0.023 ± 0.003	0.89	15.41 ± 0.25	1.9 ^{+0.8} _{-1.2}	4.8 ^{+1.1} _{-0.6}

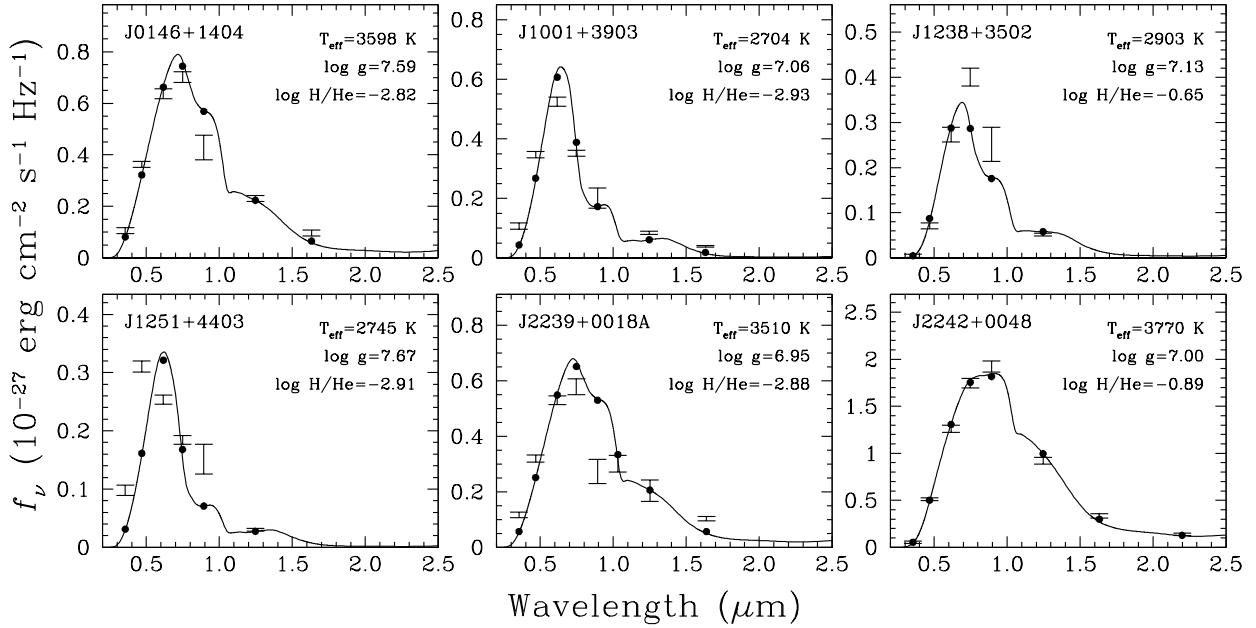


Figure 6. Fits to the SEDs of the six ultracool DC WDs in our sample. All objects have featureless spectra near the H α region, and the SEDs are best explained with mixed model atmospheres. Note that the measured abundances are quoted relative to the dominant atmospheric constituent.

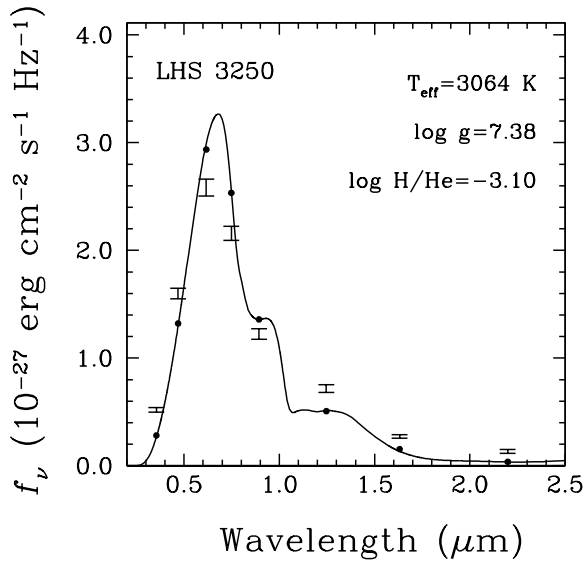


Figure 7. Similar to Fig. 6 but for the ultracool WD LHS 3250.

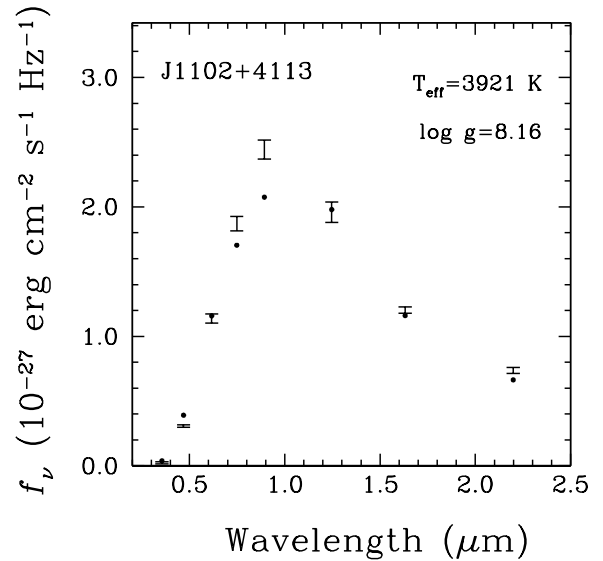


Figure 8. Similar to Fig. 4 but for the ultracool WD J1102+4113 where we show the pure H solution only.

5.2 The Nature of Ultracool WDs

The colour-magnitude diagram presented in Fig. 2 shows that the faintest WDs in our sample have $M_r \leq 16.4$ mag. This magnitude limit corresponds to WD cooling ages of 11 Gyr for $0.6 M_{\odot}$ CO-core and pure H atmosphere WDs. There are six ultracool WDs in our sample with best-fitting temperatures of < 4000 K. Constraining the nature, including the total ages of these stars, has been problematic.

Previously, Oppenheimer et al. (2001), Bergeron, Leggett & Ruiz (2001), and Kilic et al. (2012)

presented detailed model atmosphere analysis of three ultracool WDs with parallax measurements. WD 0346+246 is a 3650 K, $\log g = 8.3$ mixed atmosphere WD with $\log(\text{He}/\text{H}) = 0.43$, whereas J1102 is best explained by a pure H atmosphere model with $T_{\text{eff}} = 3830$ K and $\log g = 8.08$ (Kilic et al. 2012). These two ultracool WDs have masses of 0.77 and $0.62 M_{\odot}$, respectively. Their total main-sequence + WD cooling ages and their kinematic properties indicate Galactic halo membership. LHS 3250 stands out in this sample. Bergeron & Leggett (2002) find

a best-fitting solution of $T_{\text{eff}} = 3042$ K, $\log g = 7.27$, and $\log(\text{H}/\text{He}) = -2.7$. Fig. 7 shows our model fits to the LHS 3250 SED. Including the red wing of the Ly α opacity (Kowalski & Saumon 2006), we now derive slightly different parameters of $T_{\text{eff}} = 3064$ K, $\log g = 7.38$, and $\log(\text{H}/\text{He}) = -3.1$. Even though the models predict deep absorption features around 0.8 and 1.1 μm , these features have never been observed in the actual spectra of cool and ultracool WDs. Clearly, the models have problems (likely due to problems with CIA calculations). Nevertheless, LHS 3250 is too bright compared to the pure H atmosphere models for ultracool WDs (see Fig. 2), but its location in the colour-magnitude diagram and its SED are consistent with low surface gravity, mixed H/He atmosphere WDs.

Fig. 8 shows our model fits to the J1102 SED using pure H atmosphere models. We find $T_{\text{eff}} = 3921$ K and $\log g = 8.16$ for this ultracool WD. These parameters are consistent with the analysis based on the Kowalski & Saumon (2006) models within the errors (Kilic et al. 2012). Both Kowalski & Saumon (2006) and Bergeron, Saumon & Wesemael (1995) models underpredict the flux in the i and z bands for this star. Addition of He provides a significantly better fit to the SED. The best-fitting mixed atmosphere model has trace amounts of helium with $T_{\text{eff}} = 3327$ K, $\log g = 7.64$, and $\log(\text{He}/\text{H}) = -3.51$. Based on this, all three of the previously analysed ultracool WDs with parallax measurements would be best explained by mixed H/He atmosphere models.

The six ultracool WDs in our sample (see Fig. 6) are all similar to LHS 3250. They are overluminous compared to pure H atmosphere WDs, and their SEDs and locations in colour-magnitude diagrams are matched fairly well by mixed H/He atmosphere WD models. The models have problems matching the peaks of the energy distributions and they predict absorption features at 0.8 and 1.1 μm that are not observed, but the overall fits are quite reasonable. Based on these, all nine (including the six in our sample) ultracool WDs with parallax measurements are best explained with H-rich (mixed) atmospheres. In addition, seven of the nine are low-mass objects with He-cores. These low-mass objects are about twice as large (see Table 4), and therefore four times as bright, as typical 0.6 M_{\odot} WDs. Hence, their overabundance in the SDSS sample is not surprising.

5.3 Common Proper Motion Pairs

There are three common proper motion pairs in our sample. These include two WD + WD pairs (J0747+2438 and J2239+0018) and one WD + K dwarf (J0045+1420). The latter was reported as a common proper motion binary by Luyten (1987) and Lépine & Bongiorno (2007). LSPM J0045+1421 (BD+13 99) is a G8V star 62.5 arcsec away from LSPM J0045+1420. We confirm that both the WD (J0045+1420) and the G8 dwarf are at the same distance, making it a Sirius-like binary. Such binary systems can be used to constrain the initial-final mass relation. However, J0045+1420 is a $0.43 \pm 0.07 M_{\odot}$ low mass WD with a cooling age of 2.7 Gyr. Due to its low-mass, J0045+1420 may itself be an unresolved binary, and it is impossible to constrain its total age or the mass of its progenitor star.

The remaining two WD + WD systems are also very useful as they provide a test of our cooling age estimates.

J0747+2438 contains a $2.5^{+0.5}_{-0.3}$ Gyr old, $0.54 \pm 0.05 M_{\odot}$ DA WD and a $4.5^{+1.1}_{-0.9}$ Gyr old, $0.47 \pm 0.05 M_{\odot}$ DC WD that is best-fitted by a pure He atmosphere model. The separation between the two WDs is ≈ 2000 au; it is safe to assume that both stars evolved independently. The cooling ages of the two stars differ by $\approx 2\sigma$, and this difference could be due to a difference in the mass of the progenitor main-sequence stars, though the lower mass star (J0747+2438N) is also the older star in this system. The progenitor stars of these relatively low-mass WDs were likely Sun-like stars that lived for 10 Gyr, and J0747+2438 is probably a very old binary system in the Galactic thick disc (it has a tangential velocity of only 38 ± 2 km s $^{-1}$).

J2239+0018 consists of a $T_{\text{eff}} = 4420 \pm 90$ K cool WD with a $T_{\text{eff}} = 3510 \pm 220$ K ultracool WD companion. The two WDs are separated by only 1.85 arcsec, which corresponds to a physical separation of 155 au. Unfortunately, the relatively large error in our parallax measurement translates into a large error in mass and cooling age estimates for this binary. J2239+0018B has a cooling age of $6.3^{+7.2}_{-3.4}$ Gyr, whereas the ultracool WD J2239+0018A has a cooling age of $5.2^{+3.7}_{-1.5}$ Gyr. Given the large errors, these two estimates are consistent within the errors. Further insight into understanding similar binary systems will require more accurate distance measurements than those currently available.

5.4 Disc versus halo

Fig. 9 shows the mass versus temperature distribution of our parallax sample along with the theoretical isochrones for WDs with CO core compositions and thick envelopes, i.e., $q(\text{He}) = 10^{-2}$ and $q(\text{H}) = 10^{-4}$. Bergeron, Leggett & Ruiz (2001) explain the observed trend in the isochrones. The general trend is that low-mass WDs evolve (cool) faster than their counterparts, except that the onset of crystallization in the most massive WDs shortens the cooling times considerably. This leads to the parabola shaped isochrones. We also show the corresponding isochrones for the total main-sequence + WD cooling ages for $\tau \geq 2$ Gyr. We simply assume $t_{\text{MS}} = 10(M_{\text{MS}}/M_{\odot})^{-2.5}$ Gyr and $M_{\text{MS}}/M_{\odot} = 8 \ln[(M_{\text{WD}}/M_{\odot})/0.4]$ (Wood 1992; Leggett, Ruiz & Bergeron 1998).

The oldest globular clusters in the halo are currently producing 0.53 M_{\odot} WDs (Hansen et al. 2007). There are several WDs in our sample with $M \approx 0.53 M_{\odot}$. J1436+4332 is an excellent example of a potentially very old star. This DC WD is a $T_{\text{eff}} = 4630 \pm 30$ K, $\log g = 7.88$, $M = 0.50 \pm 0.03 M_{\odot}$ He-atmosphere WD with a WD cooling age of 5.4 ± 0.6 Gyr. Its progenitor main-sequence star was most likely a Sun-like star, with a main-sequence lifetime of 10 Gyr. Hence, the total main-sequence + WD age of J1436+4332 could be as much as the age of the Universe.

Fig. 9 demonstrates that WDs with $M < 0.5 M_{\odot}$ cannot have CO cores and also form through single star evolution within the lifetime of the Universe. Hence, they must be either He-core WDs or unresolved double degenerate systems. In fact, the majority of the targets in our parallax programme, including all of the ones with $T_{\text{eff}} \leq 4300$ K, seem to be low-mass WDs with $M < 0.5 M_{\odot}$. The isochrones shown in this figure are not appropriate for these low-mass WDs. Based on the Althaus, Serenelli & Benvenuto (2001) models, they have cooling ages ranging from 2.9 to 9.7 Gyr. Since

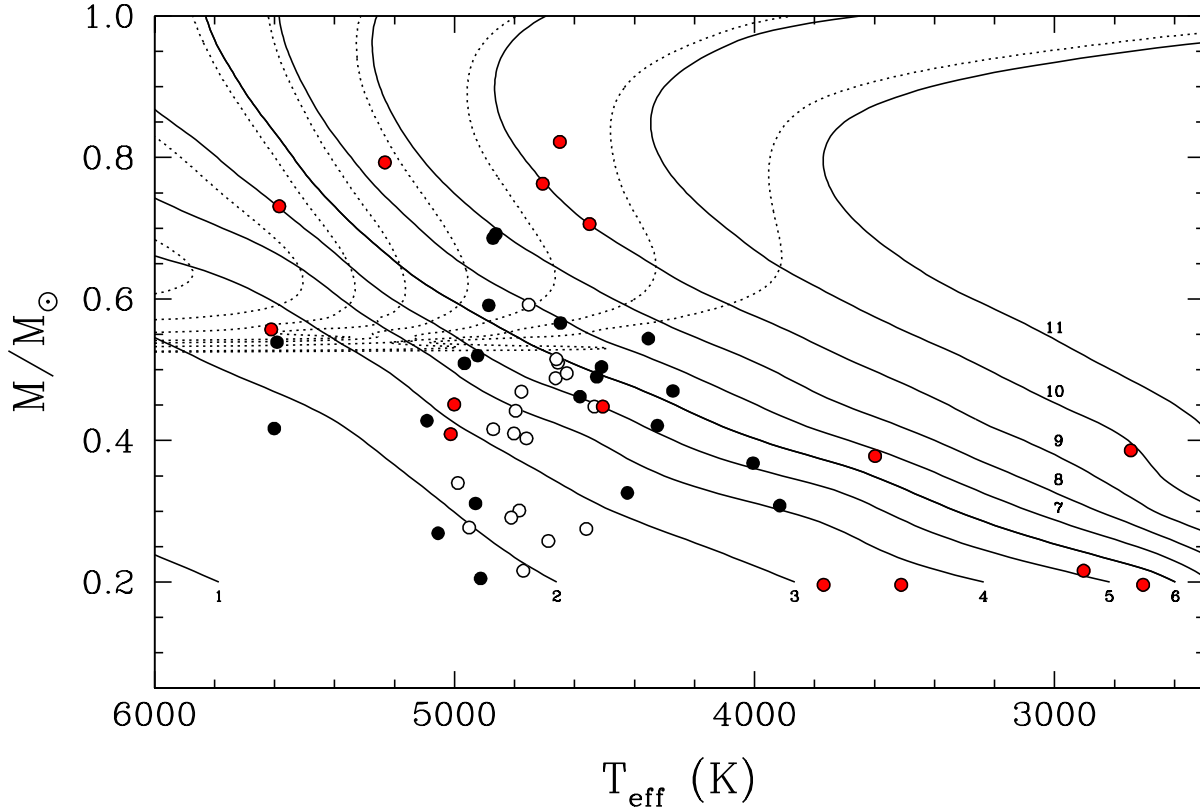


Figure 9. Masses of all stars in our sample as a function of effective temperature. The black dots correspond to the WDs with H-rich atmospheres while the white dots represent the He-rich WDs. The red dots represent the 15 cool and ultracool WDs with mixed atmospheres. Also shown are theoretical isochrones with their ages labelled in Gyr; solid lines correspond to WD cooling ages only, while the dotted lines also include the main-sequence lifetime.

the prior evolution of these systems, including the masses of their main-sequence progenitors, is unknown, their total ages cannot be estimated. However, some of the low-mass ultracool WDs are clearly very old.

Tables 2 and 4 and Fig. 10 present tangential velocities and cooling ages for our parallax sample. The cooling ages range from about 2 to 10 Gyr, whereas the tangential velocities of all but two of the targets are less than 150 km s^{-1} . The only targets that display halo kinematics are J0301–0044 and J1107+4855 (hereafter J0301 and J1107, respectively). J0301 and J1107 have tangential velocities of $167\text{--}192 \text{ km s}^{-1}$, $T_{\text{eff}} \approx 4500 \text{ K}$, $M = 0.45\text{--}0.50 M_{\odot}$ and WD cooling ages of 5–6 Gyr. If both stars are single CO core WDs, their progenitors would be Sun-like stars with main-sequence lifetimes of 10 Gyr. Hence, their total main-sequence + WD cooling ages would be ~ 14 Gyr, which is consistent with a halo origin.

In Table 2, the last three columns list the (U, V, W) components of the space velocities for each WD. These space velocities have been computed by combining the observed parallaxes and proper motions for each WD using the prescription of Johnson & Soderblom (1987). Since we do not have any radial velocity measurements for our WDs, we assume a radial velocity $v_{\text{rad}} = 0 \text{ km s}^{-1}$ in the calculation of U . In Fig. 11, we plot the resulting W versus V (top), and U versus V (bottom) velocity distributions. We also include the 2σ contours for the Galactic thin disc (dotted), thick disc (dashed) and stellar halo populations (solid) (Chiba & Beers

2000). It is clear from Figure 11 that both J0301 and J1107 are most likely halo WDs. The distribution of the remaining sample, including the IR-faint (the DC WDs with mixed H/He atmospheres) and ultracool WDs, is consistent with disc membership. The ratio of thick to thin disc WDs is 18/34. If we assume that J0301 and J1107 are indeed bona fide members of the halo, the observed velocity distribution suggests 63 per cent/33 per cent/4 per cent proportions for the contribution of thin disc, thick disc and halo WDs for our sample.

We note that this is the first time a large number of ultracool WDs have distance and tangential velocities available, and in contrast to the expectations, they all seem to be members of the disc. These WDs provide an independent constraint on the thick disc population; the Galactic thick disc is at least 10 Gyr old.

6 CONCLUSIONS

We present parallax observations of 54 cool and ultracool WDs. Our sample includes one new WD within the local 25 pc sample and five stars within 30 pc. All but two of them have tangential velocities smaller than 150 km s^{-1} . J0301–0044 and J1107+4855 are the only objects in our sample with kinematics and ages that are consistent with halo WDs. The rest of the objects, including the ultracool WDs, are members of the Galactic thick disc. The oldest

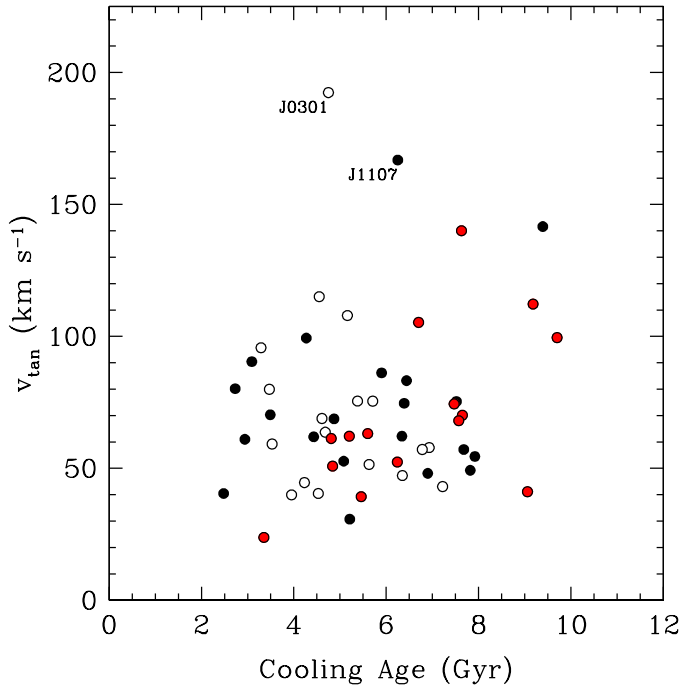


Figure 10. The tangential velocity, v_{tan} , plotted as a function of the WD cooling age. The black dots correspond to the WDs with H-rich atmospheres while the white dots represent the He-rich WDs. The red dots represent the 15 cool and ultracool WDs with mixed atmospheres.

WDs in this sample have WD cooling ages of 10 Gyr, providing a firm lower limit to the age of the thick disc. Many of our targets are low-mass WDs. These are either single He-core WDs or unresolved double degenerates. It appears that we have detected the brighter population of cool and ultracool WDs in the solar neighbourhood, and the fainter, normal CO core ultracool WDs remain to be discovered in large numbers. Future and upcoming astrometric surveys such as the LSST will find those fainter and more massive ultracool WDs.

ACKNOWLEDGMENTS

We would like to thank the anonymous referee for a careful reading of our manuscript and several constructive comments that helped improve this paper. We thank Hugh C. Harris for useful discussions and suggestions. AG acknowledges support provided by NASA through grant number HST-GO-13319.01 from the Space Telescope Science Institute, which is operated by AURA, Inc., under NASA contract NAS 5-26555. MK gratefully acknowledges support from the NSF and NASA under grants AST-1312678 and NNX14AF65G, respectively. JRT acknowledges support from the NSF under grants AST-0708810 and AST-1008217. This work was supported in part by the NSERC Canada and by the Fund FRQ-NT (Québec). This research makes use of the SAO/NASA Astrophysics Data System Bibliographic Service. This project makes use of data products from the SDSS, which has been funded by the Alfred P. Sloan Foundation, the Participating Institutions, the National Science

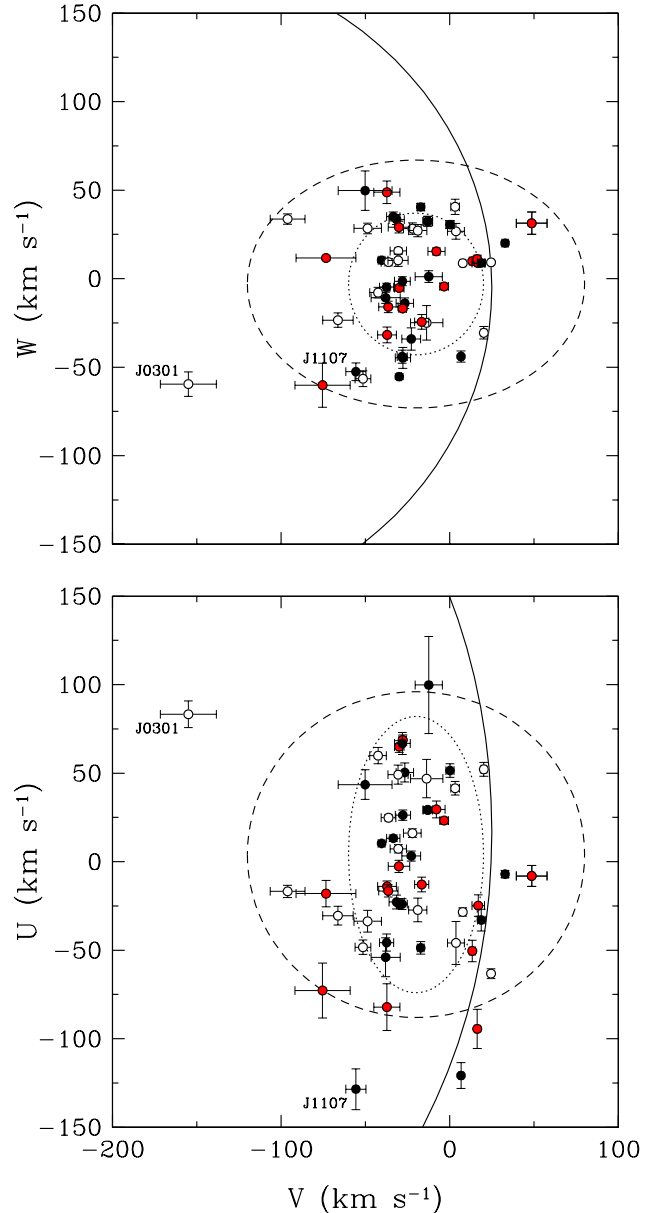


Figure 11. W versus V (top) and U versus V (bottom) velocity distributions for the 54 WDs in our sample. The ellipsoids denote the 2σ contours for the Galactic thin-disc (dotted), thick-disc (dashed) and stellar halo populations (solid). The black dots correspond to the WDs with H-rich atmospheres while the white dots represent the He-rich WDs. The red dots represent the 15 cool and ultracool WDs with mixed atmospheres.

Foundation, and the US Department of Energy Office of Science.

REFERENCES

- Ahn C. P. et al., 2014, *ApJS*, 211, 17
- Althaus L. G., Serenelli A. M., Benvenuto O. G., 2001, *MNRAS*, 323, 471
- Bergeron P., Leggett S. K., 2002, *ApJ*, 580, 1070
- Bergeron P., Leggett S. K., Ruiz M. T., 2001, *ApJS*, 133, 413

- Bergeron P., Ruiz M. T., Leggett S. K., 1997, *ApJS*, 108, 339
- Bergeron P., Saumon D., Wesemael F., 1995, *ApJ*, 443, 764
- Bergeron P. et al., 2011, *ApJ*, 737, 28
- Bohlin R. C., Gilliland R. L., 2004, *AJ*, 127, 3508
- Brown J. M., Kilic M., Brown W. R., Kenyon S. J., 2011, *ApJ*, 730, 67
- Catalán S. et al., 2012, *A&A*, 546, L3
- Chiba M., Beers T. C., 2000, *AJ*, 119, 2843
- Fontaine G., Brassard P., Bergeron P., 2001, *PASP*, 113, 409
- Gates E. et al., 2004, *ApJ*, 612, L129
- Giammichele N., Bergeron P., Dufour P., 2012, *ApJS*, 199, 29
- Hall P. B., Kowalski P. M., Harris H. C., Awal A., Leggett S. K., Kilic M., Anderson S. F., Gates E., 2008, *AJ*, 136, 76
- Hambly N. C., Smartt S. J., Hodgkin S. T., Jameson R. F., Kemp S. N., Rolleston W. R. J., Steele I. A., 1999, *MNRAS*, 309, L33
- Hansen B. M. S., 1999, *ApJ*, 520, 680
- Hansen B. M. S. et al., 2007, *ApJ*, 671, 380
- Hansen B. M. S. et al., 2004, *ApJS*, 155, 551
- Harris H. C., Dahn C. C., Vrba F. J., Henden A. A., Liebert J., Schmidt G. D., Reid I. N., 1999, *ApJ*, 524, 1000
- Harris H. C. et al., 2008, *ApJ*, 679, 697
- Harris H. C. et al., 2006, *AJ*, 131, 571
- Holberg J. B., Bergeron P., 2006, *AJ*, 132, 1221
- Holberg J. B., Sion E. M., Oswalt T., McCook G. P., Foran S., Subasavage J. P., 2008, *AJ*, 135, 1225
- Hummer D. G., Mihalas D., 1988, *ApJ*, 331, 794
- Iben, Jr. I., Tutukov A. V., 1984, *ApJ*, 282, 615
- Ivezic Z. et al., 2008, preprint (arXiv:0805.2366)
- Johnson D. R. H., Soderblom D. R., 1987, *AJ*, 93, 864
- Kilic M. et al., 2010, *ApJS*, 190, 77
- Kilic M. et al., 2006, *AJ*, 131, 582
- Kilic M., Thorstensen J. R., Kowalski P. M., Andrews J., 2012, *MNRAS*, 423, L132
- Kowalski P. M., Saumon D., 2006, *ApJ*, 651, L137
- Lawrence A. et al., 2007, *MNRAS*, 379, 1599
- Leggett S. K., Lodieu N., Tremblay P.-E., Bergeron P., Nitta A., 2011, *ApJ*, 735, 62
- Leggett S. K., Ruiz M. T., Bergeron P., 1998, *ApJ*, 497, 294
- Lépine S., Bongiorno B., 2007, *AJ*, 133, 889
- Lépine S., Shara M. M., 2005, *AJ*, 129, 1483
- Liebert J., Dahn C. C., Monet D. G., 1988, *ApJ*, 332, 891
- Luyten W. J., 1987, *Proper Motion Survey with Schmidt Telescopes*, 71, 1
- Marsh T. R., Dhillon V. S., Duck S. R., 1995, *MNRAS*, 275, 828
- Mestel L., 1952, *MNRAS*, 112, 583
- Munn J. A. et al., 2004, *AJ*, 127, 3034
- Oppenheimer B. R. et al., 2001, *ApJ*, 550, 448
- Perryman M. A. C. et al., 2001, *A&A*, 369, 339
- Press W. H., Flannery B. P., Teukolsky S. A., Vetterling W. T., 1986, *Numerical Recipes*
- Rowell N. R., Kilic M., Hambly N. C., 2008, *MNRAS*, 385, L23
- Sion E. M., Holberg J. B., Oswalt T. D., McCook G. P., Wasatonic R., Myszka J., 2014, *AJ*, 147, 129
- Skrutskie M. F. et al., 2006, *AJ*, 131, 1163
- Thorstensen J. R., 2003, *AJ*, 126, 3017
- Thorstensen J. R., Lépine S., Shara M., 2008, *AJ*, 136, 2107
- Tokunaga A. T., Simons D. A., Vacca W. D., 2002, *PASP*, 114, 180
- Tremblay P.-E., Bergeron P., 2009, *ApJ*, 696, 1755
- Tremblay P.-E., Leggett S. K., Lodieu N., Freytag B., Bergeron P., Kalirai J. S., Ludwig H.-G., 2014, *ApJ*, 788, 103
- Vidrih S. et al., 2007, *MNRAS*, 382, 515
- Winget D. E., Hansen C. J., Liebert J., van Horn H. M., Fontaine G., Nather R. E., Kepler S. O., Lamb D. Q., 1987, *ApJ*, 315, L77
- Wood M. A., 1992, *ApJ*, 386, 539

This paper has been typeset from a \TeX / \LaTeX file prepared by the author.